Journal Pre-proofs

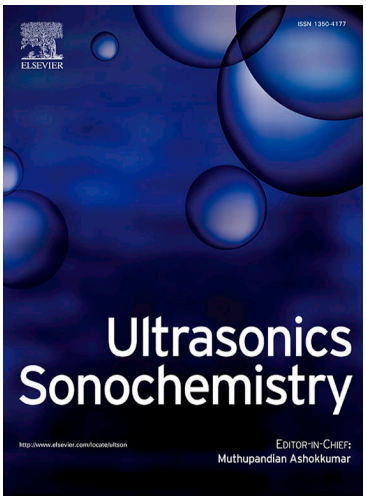

Recent progress on sonochemical production for the synthesis of efficient photocatalysts and the impact of reactor design

Panayiota Adamou, Eleana Harkou, Sanaa Hafeez, George Manos, Alberto Villa, S.M. Al-Salem, Achilleas Constantinou, Nikolaos Dimitratos

PII: S1350-4177(23)00322-X
DOI: https://doi.org/10.1016/j.ultsonch.2023.106610
Reference: ULTSON 106610

To appear in: *Ultrasonics Sonochemistry*

Received Date: 25 July 2023
Revised Date: 18 September 2023
Accepted Date: 19 September 2023

Please cite this article as: P. Adamou, E. Harkou, S. Hafeez, G. Manos, A. Villa, S.M. Al-Salem, A. Constantinou, N. Dimitratos, Recent progress on sonochemical production for the synthesis of efficient photocatalysts and the impact of reactor design, *Ultrasonics Sonochemistry* (2023), doi: https://doi.org/10.1016/j.ultsonch.2023.106610

Recent progress on sonochemical production for the synthesis of efficient photocatalysts and the impact of reactor design

Authors

Panayiota Adamou[1,†], Eleana Harkou[1,†], Sanaa Hafeez[2], George Manos[3], Alberto Villa[4], , S.M. Al-Salem[5], Achilleas Constantinou[1,*] Nikolaos Dimitratos[6,7*]

[1] Department of Chemical Engineering Cyprus University of Technology, 57 Corner of Athinon and Anexartisias, 3036 Limassol, Cyprus.

[2] School of Engineering and Materials Science, Queen Mary University of London, London, E1 4NS, United Kingdom.

[3] Department of Chemical Engineering, University College London, London WCIE 7JE, UK.

[4] Dipartimento di Chimica, Universitá degli Studi di Milano, via Golgi, 20133 Milan, Italy.

[5] Environment & Life Sciences Research Centre, Kuwait Institute for Scientific Research, P.O. Box: 24885, Safat 13109, Kuwait.

[6] Department of Industrial Chemistry "Toso Montanari", University of Bologna, viale Risorgimento 4 40136 Bologna, Italy.

[7] Center for Chemical Catalysis – C3, University of Bologna, viale Risorgimento 4 40136 Bologna, Italy.

Corresponding authors:

Nikolaos Dimitratos, email: nikolaos.dimitratos@unibo.it

Achilleas Constantinou, email: a.konstantinou@cut.ac.cy

[†] These authors share first authorship.

Abstract

Sonochemical-assisted synthesis has flourished recently for the design of photocatalysts. The main power used is ultrasound that allows the nanomaterials shape and size modification and control. This review highlights the effect in formation mechanism by ultrasound application and the most common photocatalysts that were prepared via sonochemical techniques. Moreover, the challenge for the suitable reactor design for the synthesis of materials or for their photocatalytic evaluation is discussed since the most prominent reactor systems, batch, and continuous flow, has both advantages and drawbacks. This work summarises the significance of sonochemical synthesis for photocatalytic materials as a green technology that needs to be further investigated for the preparation of new materials and the scale up of developed reactor systems to meet industrial needs.

1. Introduction

Recently, an increasing amount of effort has been to overcome arising environmental problems such as pollution from the extensive use of conventional fuels and global energy crisis. Green chemistry or sustainable chemistry revolves around the design of environmentally friendly methods for the development of greener reactions, restricting the use of dangerous substances. Therefore, green chemistry's principles were founded to provide sustainable approaches for the design of new processes and products and also eliminate hazard organic pollutants and heavy metals [1], [2].

Green technology revolves around two main strategies: green process innovation and green product innovation. The main objective of the former is to contribute to the design of products reducing the use of nontoxic compounds and increasing the use of natural sources [3]. The aim of the latter is to improve the life cycle of a product from the beginning till the end (e.g., cradle to grave). This includes the use of recyclable materials and reduction of hazardous substances. Most of these methods such as ball milling, sol-gel, and spray pyrolysis are expensive, consumes high energy with an extended operational time [4]. Therefore, is a necessity to not only decrease time and energy consumption but also to find methods with higher efficiency and less environmentally burdensome.

Sonochemistry is a promising green field that investigates the ultrasonic waves application for the promotion of chemical processes and material synthesis. The ultrasound irradiation utilisation compared to the conventional methods, results in less reaction time, higher selectivity and nanoparticles (NPs) with modified morphology and properties. Ultrasonic

waves can be applied in different processes such as waste treatment, analytical chemistry, materials chemistry, and nanocatalyst synthesis [5]. Therefore, sonochemistry is a field with multiple applications and of significant importance since ultrasonic waves form acoustic cavitation in solutions that enhances chemical activity with a high economical value. There is a plethora of types of NP and nanostructured materials that can be produced by sonochemical synthesis such as noble metals, transition metals, semiconductors, carbon materials and polymeric materials [6]. On the other hand, the sonochemical methods have some drawbacks such as transducers surface erosion in continuous operations [7], as their scalability is considered limitation due to the lack of continuous flow synthesis of NP in literature [8] and the yield of the reaction is affected negatively [9].

One of the various applications of such is photocatalysts' sonochemical synthesis. The combination of light irradiation and ultrasonic waves in heterogeneous catalysis is a technique that is used for the preparation of active and efficient photocatalysts [10]. An extensive amount of research has been conducted for the synthesis of different photocatalysts utilising sonochemical methods and many of them were related to environmental remediation applications, focusing on wastewater treatment for the decomposition of hazardous and toxic substances and for the removal of dyes [11]–[30]. Therefore, there is a great need to develop novel catalysts by applying ultrasonic waves created by the ultrasounds to act as a source of energy to convert the reactants to products in ways that do not occur otherwise.

This review addresses the benefits of utilising ultrasound waves to synthesise photocatalysts. The principals of sonochemistry are highlighted, as well as, the mechanisms in synthesising different materials. Afterwards, examples of the most studied photocatalysts prepared by sonochemistry and how this method benefits their synthesis are discussed. Lastly, different reactor types that were applied for the photocatalytic experiments to evaluate the photocatalysts performance are mentioned. In the literature it was found that most of the studies investigating different reactor designs focus either on batch or on microreactors [31]–[33]. This review study, pays attention to novel sonochemical synthesis of materials, promoting green and sustainable chemistry, focuses on recent developments of reactors used for synthesis and photocatalytic experiments, whilst highlighting gaps for further research and development.

2. Principles of Sonochemistry

The scientific field of sonochemistry focuses on investigating the effects and practical applications of high-frequency sound waves [34]. Ultrasound, which is a longitudinal wave type with an exceeding 20 kHz (20,000 cycles per second) frequency, surpasses the upper human auditory perception limit. The ultrasound introduction into a liquid exerts alternating compression and expansion cycles on the liquid, generating positive and negative pressure respectively [35], [36]. This process leads to the formation of cavitations (bubbles), which are essentially voids or cavities that arise from existing impurities and undergo oscillation in response to the applied sound waves. As the bubbles grow over few cycles and accumulate

ultrasonic energy, they trap vapour (such as water vapour, dissolved gases, and volatile organic substances) from the surrounding medium, reaching a critical size typically in the range of tens of micrometers, before ultimately collapsing [36].

Once a bubble is generated, two cavitation types of phenomena can occur: stable or transient. Under low-intensity, it is observed high-frequency ultrasonication (greater than 50 kHz), stable cavitation whereas, the wall of bubble couples with the oscillating acoustic field around its equilibrium radius for several cycles. Quasi-reversible it is considered inside the bubbles, the solvent evaporation and condensation in this regime. Nevertheless, rectified diffusion can take place, causing trap for some of the vapour some within the cavity due to variations in mass transfer rates across its interface. This trapped vapour leads to bubble growth [37]. The bubble continues to expand gradually until it reaches its critical size, at a point energy, from the sound field, can not be efficiently absorbed to sustain its growth, becoming unstable [36].

In the other case where high-intensity, low-frequency ultrasonication (e.g., 20–50 kHz) is applied to the liquid, it is commonly obtained transient cavitation. In this case, the produced bubbles undergo rapid and excessive expansion due to inertia, causing their size to increase dramatically compared to the equilibrium radius, followed by eventual collapse [38]. Significant is the solvent vapour evaporation within the bubble during the expansion phase [39]. Upon collapse, the stored concentrated energy within the bubble is rapidly released in a short time, resulting of approximately 5000 K extremely localised and transient temperatures and about 1000 bar pressures, according to the thermal "hot spot" theory [40].

The created environment through the acoustic cavitation offers opportunities for synthesising novel materials that are often unattainable using other methods. The extreme conditions resulting from bubble implosion enable syntheses to be carried out at room temperature in liquid solutions, which would typically require high temperatures and pressures, and prolonged reaction times. Using ultrasonic irradiation for nanomaterials preparation, the phenomena that contribute to sonochemistry are classified into primary sonochemistry, secondary sonochemistry, and physical modifications [41].

Primary sonochemistry is well known for the formation of hotspot that enables the production of extraordinary materials. The reaction occurs inside the bubble among precursor ions and different chemicals. Primary sonochemistry favours reactions such as hydrothermal or solvothermal for the synthesis of nanomaterials. Secondary sonochemistry allows scattered ions and radicals to diffuse into liquid phase and interact with the solution, followed by material synthesis. Therefore, the reactions take place outside from the bubble avoiding any physical force. Physical effects occur from intense shock waves and/or high-speed jets induced by cavitation [42]. It is crucial to emphasise the physical and chemical ultrasound effects are not a result of direct interactions between sound waves and chemical species. Rather, they arise from the bubbles formation, growth, and collapse [41].

3. Formation mechanisms by sonochemistry application

Comparing with conventional methods ultrasound-assisted methods are valuable to accelerate chemical reactions, creating a new phase and influence the structure and surface of the

synthesised particles through the acoustic cavitation. When sonochemistry is applied for the synthesis of catalysts, shape and size are modified [43]–[46]. Moreover, this technique obstruct clusters' agglomeration, resulting in high and stable dispersion of micro- and meso-sized particles [47]. The control of particle sizes can easily be achieved by varying reagents concentration and herein the reaction rate. Kim et al. [48] showed the molar ratio effect of reactants on the silica particle size. Test samples were prepared varying the TEOS:C_2H_5OH:H_2O:NH_4OH molar ratio and uniform and monodispersed silica particles were synthesised. The increase of molar ratio of ammonia, from 2.85 to 8.54, led to the increase of particle size, from approximately 285 to 430 nm, attributed to the change of reaction rate controlled by the silica catalyst in the process. In contrast, the decrease of water's molar ratio, from 61.6 to 12.4, at different NH_4OH ratios showed decrease in the particle size of synthesized silica particles, from about 285 to 39 nm for NH_4OH molar ratio of 2.85 and from 316 to 110 nm for NH_4OH molar ratio of 5.7. Also, it was observed that the average particle size was controllable within the range of 40 and 400 nm. Additionally, more ultrasonic parameters were observed from different works to affect the size of NPs including the ultrasonic frequency, the type of reagents, alcohols and surfactants and the atmospheric gases [49].

Wang et al. [50] synthesised nanocomposites of ZrO_2-Al_2O_3/GO utilising a sonochemical method to effectively remove fluoride (F^-). The NPs of ZrO_2 and Al_2O_3 were quickly formed without the use of precipitation and quickly forming metal oxide NPs. A higher adsorption capacity was observed by the sonochemical prepared adsorbents than those created by co-precipitation methods. As it can be seen from the figure below (Figure 1), a 3D network is formed via ultrasonication, providing higher surface area with smaller pore size and higher pore volume. XPS analysis confirmed that metal oxide NPs result in stronger interaction with F^-. Based on these results, it is evident that the sonochemical method promotes the performance of the adsorbents.

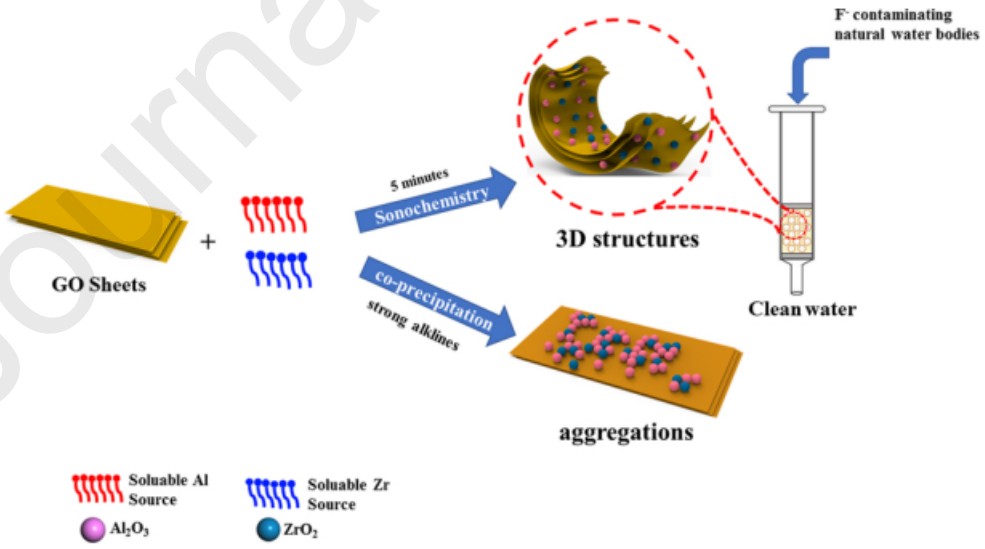

Figure 1. Mechanism followed to synthesise ZrO_2-Al_2O_3/GO with sonochemistry and co-precipitation [50].

TiO_2-P25-CuO_x photocatalysts were prepared by ultrasound-assisted ultra-wet impregnation technique by Giannakoudakis et al. [51] using TiO_2 P25 as support. The aim of this synthetic method was to decorate the surface of the support homogeneously with nanoclusters of copper oxides. The synthesis protocol is depicted below (Figure 2). Ultrasonication was utilised all along the way of the synthesis (120 W, 37 kHz). After the sonication the obtained material was dried at 80 ^oC and then a calcination procedure was carried out under air at 400 ^oC for 4 h where CuO_x NPs (~ 2nm) were formed in the surface of TiO_2 P25. The obtained photocatalysts were tested for H_2 production and oxidation of 5-hydroxymethylfurfural (HMF) and benzyl alcohol (BnOH) to 2,5-diformylfuran (DFF) and benzyl aldehyde (PhCHO), respectively, achieving an enhanced and constant capability of generating H_2 and high yields of DFF and PhCHO, while TiO_2-P25 commercial catalyst revealed no H_2 formation under the same conditions and lower yields.

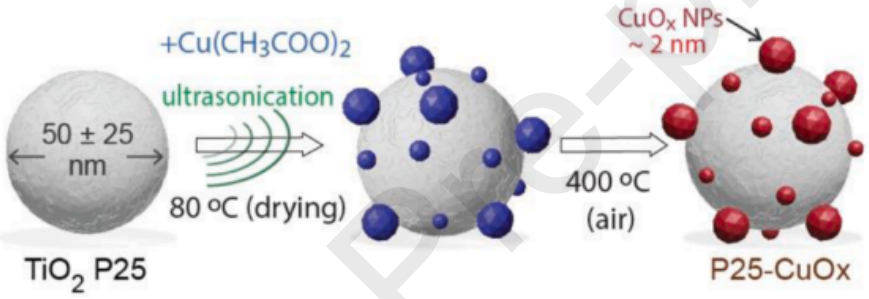

Figure 2. Design strategy of TiO_2-P25/CuO_x [51].

Optimised shapes and particle size distribution in the colloidal synthesis of Au NPs (GNPs) using ultrasonic irradiation powers of 60, 150 and 210 W (probe of 20 kHz frequency) were studied by Fuentes-García et al [52]. The temperature of the experimental setup was monitored every 10 min and the pH before and after irradiation (60 min) in order to determine how ultrasound affects the formation mechanism. Physical and chemical conditions were found to be associated with changes in size and shape of the particles. Figure 3 depicts an illustration of the mechanism followed for the nucleation and growth of the GNPs via ultrasonic irradiation. A reduction process from Au^{3+} to Au^0 assisted by the formed radicals in the solution is confirmed by UV-Vis analysis that allows Au cluster formation. The mechanism present is enhanced by the application of ultrasound and no additional stirring or heating were needed. TEM and FTT high-resolution images revealed their FCC structure. Smaller GNPs were synthesised with increasing the power of irradiation. The authors concluded that this preparation method is a great strategy to control shape and size and scalable to meet industrial criteria.

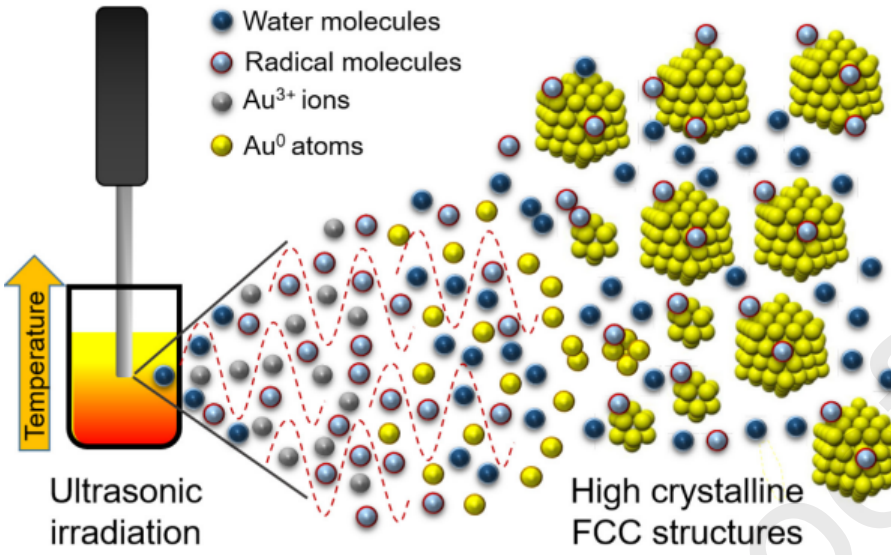

Figure 3. Nucleation and growth mechanism assisted by ultrasonic irradiation [52].

$Cu_xCe_{1-x}O_2$ nanostructures with different percentages of copper was synthesised using a single step sonochemical method by Mousavi-Kamazani and Azizi [53]. A high-intensity ultrasonic probe with a power of 40 W operating at 20 kHz was used for the sonochemical treatment. The aim of this study was to control the growth of the particles and more specifically the generation of flower-like morphology with wide sheets for better photocatalytic efficiency. A schematic diagram (Figure 4) illustrates the Cu doped CeO_2 formation with and without the ultrasonic irradiation. The effect is clear since in ultrasonic waves absence, the structure of the particles is spherical but under ultrasonic irradiation the morphology is changed. Radical species are formed in solvents under ultrasonic waves and since water was the solvent for this reaction, $^{\bullet}H$ and $^{\bullet}OH$ were generated that can interfere with Cu^{2+}, thus the reaction mechanism. Nucleation and growth mechanisms change resulting in different structure for the product. Therefore, the nanostructures prepared by sonochemistry exhibited excellent photocatalytic activity when exposed to light and were also able to remove the adsorbed colour on their surface making it dual function material.

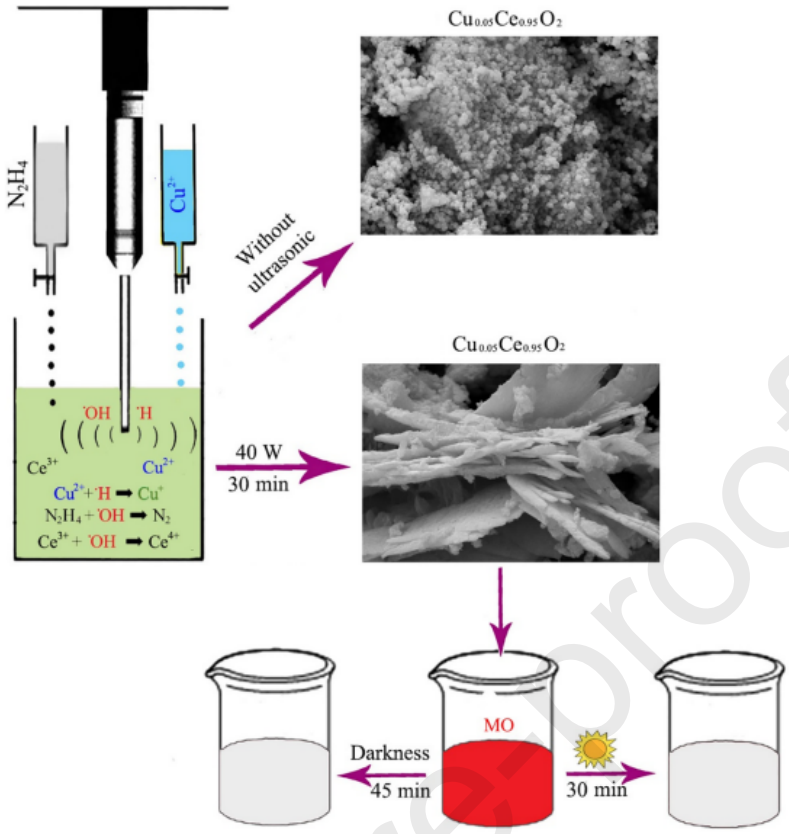

Figure 4. Different morphologies obtained with and without ultrasonic irradiation [53] .

Bahadoran et al. [54] synthesised novel Bi_2WO_6-$ZnBi_2O_4$ (BWO-ZBO) catalysts combining sonochemistry and hydrothermal treatment with different amounts of $ZnBi_2O_4$. The procedure followed is depicted at Figure 5. The two prepared were mixed under sonication for 30 min and afterwards hydrothermal treatment took place for 12 h in at 180 °C. Crystalline NPs with flat-like morphology were obtained via sonochemical treatment while the particles prepared conventionally remained spherical and amorphous. The photocatalytic degradation of Malachite Green (MG) was tested for the evaluation of the photocatalysts prepared. BWO-20ZBO (20 wt% $ZnBi_2O_4$) exhibited the best photocatalytic MG degradation (86%) compared with the others. Moreover, BWO-20ZBO catalyst without any sonochemical pre-treatment, resulted in a 72% MG degradation indicating that the changed morphology induced by acoustic cavitation improves the photocatalytic performance.

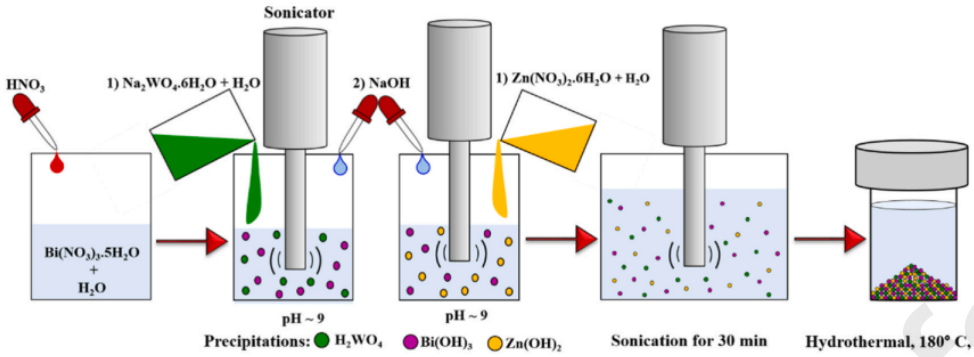

Figure 5. Synthesis procedure with sonochemical treatment [54].

4. Sonochemical Synthesis of Photocatalysts

Photocatalysts is a great example of green chemistry due to their ability to convert directly to solar energy to an easily stored H_2 and their not harmful impact on environment [55]. The utilisation of acoustic waves in the synthesis of metal NPs was initially documented by Gutierrez and Henglein [36]. Subsequently, Nagata [56] employed the technique to produce Ag NPs by reducing precursor materials. This pioneering work laid the foundation for the development of acoustic wave synthesis techniques, which have since facilitated the synthesis of various nanostructured photocatalytic materials including metal NPs and metal oxides. The following highlights some of the prominent photocatalysts prepared through the application of sonochemistry such as metal oxides, metal chalcogenides and heterojunctions. In most cases, the activity of the synthesised catalysts was investigated by the degradation of various dyes.

4.1 *Metal oxides and supported metal nanoparticles*

Numerous researchers have demonstrated the superiority of the sonochemical technique compared to conventional approaches in metal oxides and supported metal nanoparticles synthesis. This technique offers several advantages, including reduced reaction time, enhanced phase purity, increased surface area, and improved uniformity in the distribution of particle size [31]. In recent decades, there have been a notable focus on titanium dioxide (TiO_2) in the realm of air and water pollutants photocatalytic removal [57]–[65]. This is primarily attributed to its advantageous characteristics, including non-toxicity, affordability, photo-corrosion high resistance, and strong chemical and physical stability [66]. Lee and Choi [66] synthesised different Ce ratios (0.5, 0.75, 1.0, 1.5, and 2.0 wt. %) of Ce-doped TiO_2 nanostructures (CeT) using a sonochemical processing method. The synthesised CeT particles had greater surface area (~ 93-109 m2/g) and smaller particle size (~11-13 nm) than that of a pure TiO_2 (58.1 and 24.2 nm respectively). The effectiveness in photocatalysis of the synthesised CeT was evaluated by measuring their degradation efficiencies for gaseous toluene and o-xylene, which are recognised as prominent indoor air pollutants, under daylight

irradiation. The CeT samples demonstrated notably enhanced performance in toluene's and o-xylene's degradation, surpassing that of pure TiO_2 and commercial P25 TiO_2. It was concluded that simplified Ce-doped TiO_2 nanostructures sonochemical synthesis possess potential for controlling indoor air pollutants.

Nanospherical TiO_2 embedded with self-supported graphene oxide (GO) nanosheets using a low cost sonochemical method by Purkayastha et al [67]. The modified TiO_2-GO (TGO) catalysts with a 0.1 g : 0.5 g GO:TiO_2 ratio showed enhanced catalytic activity for azo dyes degradation (methyl orange (MO) and congo red (CR)), due to higher surface area (92 m^2/g) than that of bare TiO_2, reduced crystallite size of 28 nm and unique morphology and. Stability measurements showed that the photocatalyst is stable in pollutants presence at different pH levels. The catalytic performance of the photocatalyst was investigated under UV light and UV irradiation monitoring the dye decolourisation rates. The CR dye showed the highest decolourisation at neutral pH of 84 %, 30 min of irradiation time, 100 mg of photocatalyst dose and 5 mg/L of dye concentration. Moreover, the investigated catalyst was found to exhibit enhanced photosensitivity and could be reused without any activity loss, up to three consecutive cycles.

Dey and Gogate [68], investigated the effect of the synthesis method of Fe-TiO_2 and Ce-TiO_2 structures. A conventional (C) and an ultrasound assisted (US) homogeneous coprecipitation method was used and it was observed that the intensification improves the crystallinity, lowers the particle size (1270 and 1170 nm for Ce-TiO_2(C) and Fe-TiO_2(C), and 584 and 449 nm for the Ce-TiO_2(US) and Fe-TiO_2(US), respectively) and increases the surface area of the catalyst in the case of Ce-TiO_2(US) (185.65 m^2/g). Figure 6 shows the field emission scanning electron microscopic (FESEM) images, presenting the spherical shape of NPs revealing enhanced porosity of the NPs after the US synthesis. The Victoria blue dye was used to study the photocatalytic, sonocatalytic and sonophotocatalytic oxidation performance of the catalysts where it was obtained that the sonochemically synthesised Ce-TiO_2 showed maximum decolourisation around 72 % in the sonophotocatalytic approach. Additional studies revealed that the easily regeneration of catalysts with no structural changes and ions' leaching from the catalyst into the solution is negligible.

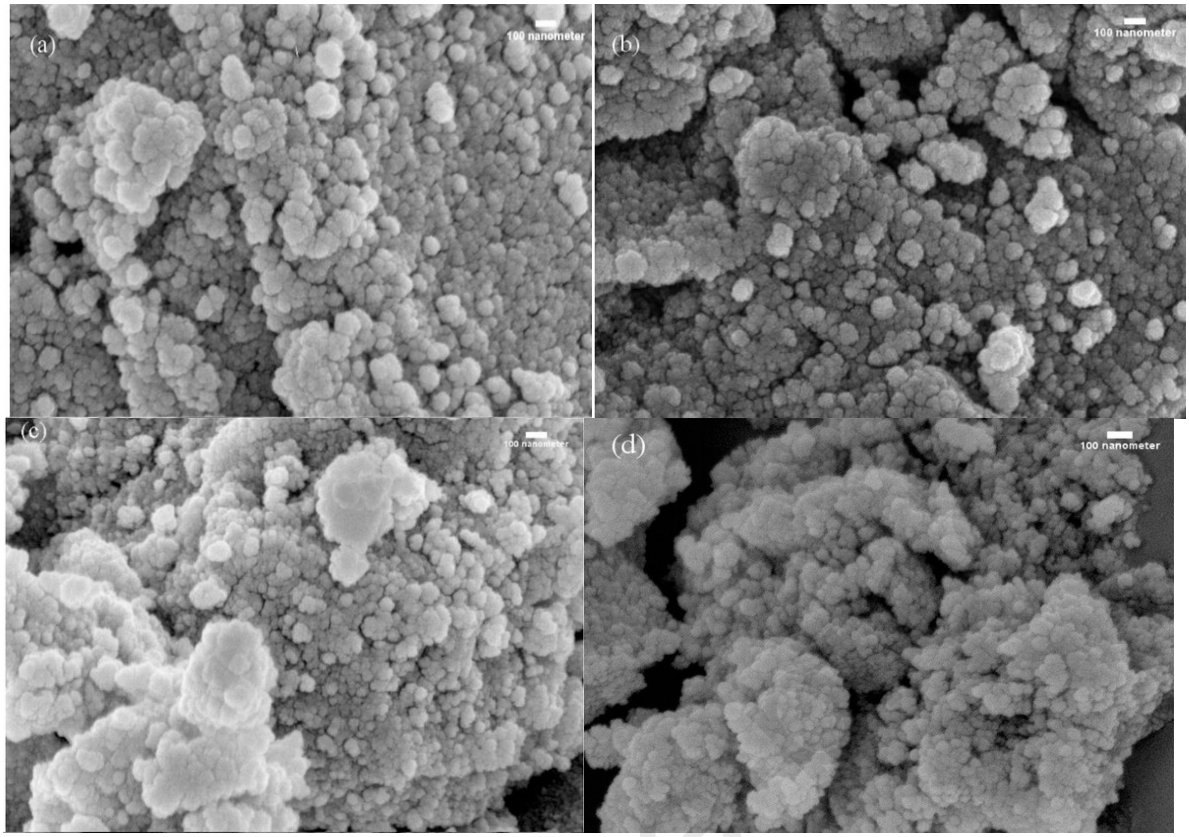

Figure 6. FESEM images of catalysts obtained using different approaches (a) Ce-TiO_2 (C), (b) Ce-TiO_2 (US), (c) Fe-TiO_2 (C), (d) Fe-TiO_2 (US) [68].

Another study by Dey et al. [69], was focused on Ce-TiO_2 nanocatalyst synthesis using sonochemical coprecipitation method. The catalytic performance of the nanocatalyst was investigated through a (i) photocatalytic, (ii) sonocatalytic, (iii) sonophotocatalytic and (iv) H_2O_2 assisted sonophotocatalytic method. The synthesised catalyst had a spherical morphology with 1.44 nm crystallite size. It was obtained that the amount of catalyst required for the sonophotocatalysis was lesser that that of photocatalysis and sonocatalysis. Moreover, the combination of sonophotocatalytic method with H_2O_2 showed the best results for chemical oxygen demand (COD) reduction of around 85 %, while the obtained results for photocatalysis, sonocatalysis and sonophotocatalysis were approximately 45, 59 and 64.5 %, respectively. It was revealed the improved mass transfer on the catalytic surface, the removal of impurities from the catalytic surface and the increased treatment efficiency by the incorporation of ultrasound waves.

Likewise the TiO_2, ZnO semiconductor is considered among the most evaluated photocatalysts due to its excellent physicochemical properties [70], technological, economical properties and eco-friendly applications [71]. Muthukrishnaraj et al. [71] synthesised a reduced graphene oxide (RGO) (1, 2, 3, 4 wt% of GO) supported on ZnO hexagonal hollow rods fabricated through sonochemical method. It was observed that the ZnO hexagonal hollow rod particles sizes decrease with the addition of the dispersed RGO sheets. The photocatalytic activity of pure ZnO and RGO doped on ZnO catalysts varying their weight percentage was assessed by using MO and methylene blue (MB) aqueous dye solutions. The 3 wt. % RGO doped on ZnO catalyst showed the highest degradation efficiency of around 91, 90 % at 180, 240 min for MB and MO respectively.

Heterostructure Pd/ZnO photocatalysts were prepared with different weight loading of Pd (1, 5, and 10 wt % of Pd) by Intaphong et al. [72], by sonochemical deposition method and were then used for MB and MO degradation. It was obtained that the metallic Pd^0 efficiently was loaded on the surface of ZnO with a particle size between 40 and 90 nm. The 5wt.% Pd/ZnO photocatalyst had the highest MB and MO photodegradation of approximately 97 and 83.5 %, respectively, under UV light irradiation within 80 min. Also, it was revealed that the Pd NPs played crucial role in the promotion of the separation of charge carriers during the photocatalytic reaction.

Shenoy et al. [73], used a novel one-pot ultrarapid sonochemical synthesis technique for copper's doped zinc oxide grafted fabrication on graphene layers ($ZnO\text{-}Cu_x\text{-}GO_y$) in order to investigate the capability of this synthesis method. Electron microscopy studies showed the ZnO hierarchical structures (HHs) growth decorated with Cu NPs and interconnected by graphene layers. The synthesised catalyst showed higher photodegradation efficiency of ibuprofen (IBU) under visible light irradiation compared to pristine ZnO HHs. The combination of the graphene and doped Cu^{2+} ions led to an enhancement of catalytic performance, due to the improvement in the visible light absorption and inhibition of the photogenerated charges recombination. This new synthesis approach can be the key for time saving and multi-component HHs scalable design of various metals.

Mousavi-Kamazani and Azizi [53], investigated the photocatalytic performance of various percentages of Cu-doped on CeO_2 nanostructures synthesised by a sonochemical method. It was also investigated the power, ultrasonic time, OH^- source, and solvent effect on the morphology of final products. The optimum synthesis method for the formation of flower-like $Cu_{0.05}Ce_{0.92}O_2$ nanostructures showed that in the darkness they had large surface for photocatalytic processes and adsorption to the solution's colour removal for about 45 min. Also, the photocatalytic activity in the light of nanostructures, removed the adsorbed colour on their surface. It is clear that the sonochemical approach of synthesising catalysts has a positive effect on the crystallinity, the particle size, the chemical and physical properties as well as to enhance photocatalytic activity.

4.2 Metal chalcogenides

The metal chalcogenide (MC) NPs have received significant attention of many scientists the recent years due to their improved properties at nanoscale making them ideal for photovoltaic applications [74]. The layer-depended bandgap of MCs and hence their excellent electronic and mechanical performance is promising with vast prospects of applications. The synthesis of MCs involves the presence of a metal precursor such as Fe, Cu, Co, Mo and Sn and a chalcogen source such as selenourea (Se) or thiourea (S) [19], [75]–[79]. Hoda and Jamali-Sheini [80], synthesised Cu_3Se_2 nanostructures with an average size less than 100 nm, in distilled water and ethanol solvent at 80 ^oC through sonochemical preparation method. Different synthesis parameters where investigated such as the molarity, the time and the ultrasonication waves' power on the properties of the photocatalyst. Characterisation studies reveal the tetragonal phase of the photocatalyst as well as the enhanced crystallinity by ultrasonic wave's power and time increasing, and by reducing the strain on the Cu_3Se_2 crystal lattice. In visible and ultraviolet regions, the higher absorption is indicating the potential applications of these nanostructures as optical sensors, solar cells, and for the photocatalytic degradation of chemical pigments in lights.

Sakthi et al. [81], reported the SnS nanocrystals ultrasonic synthesis and their performance in various applications. Structural analysis showed that the excellent nanocrystal size control was achieved with the ultrasonic synthesis for various polyvinyl pyrrolidone (PVP) quantity to be utilised as agglomeration preventing agent. The high resolution transmission electron microscopy (HRTEM) images (Figure 7) were taken in order to understand better the morphology of SnS-2 NPs, where PVP was 2g for the synthesis, indicating the narrow NPs size distribution ranging from 5 to 10 nm, and the presence of aggregates. 1.18, 1.26 and 1.34 eV band gap values, were obtained for the SnS-0, SnS-1 and SnS-2 NPs, respectively. The enhanced optical bandgap showed that the NPs were stabilised indicating the quantum confinement induced in the SnS due to the PVP stabilisation. Also, they have shown excellent supercapacitor behaviour, recyclability, and MB's photocatalytic degradation performance, under LED light illumination.

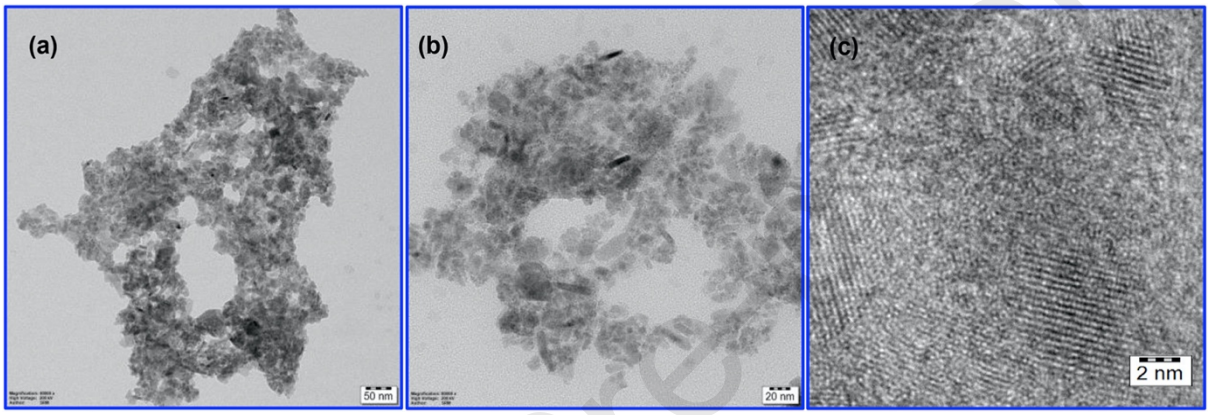

Figure 7. HRTEM images of SnS-2 NPs [81].

Khimani et al [82], investigated the sonochemically synthesised SnS_2 NPs using elemental, structural, surface and thermal analysis methods. X-ray was used to determine the structures crystallinity with the NPs to be polycrystalline and possess hexagonal structure. The crystallite size was 25.4 and 35.9 nm for the as-synthesised and thermal analysed samples, respectively. Their particle size was obtained to be almost uniform and in globular shape. In addition, by recording the thermogravimetric and differential thermogravimetric curves, the thermal analysis was carried out showing that the NPs follow three steps of decomposition and that the particles were found slightly rich in Sn while the post-thermal samples were more Sn rich, S deficient, increase of crystallite size and XRD diffraction peaks. Thermodynamic parameters such as activation energy (E_a), change in activation Gibb's free energy (ΔG^*), change in activation enthalpy (ΔH^*) and change in activation entropy (ΔS^*) were determined.

Jafarinejad et al. [83], assessed the photoactivity, in visible light, of pure and flower-like $CuInS_2$ NPs during the Eriochrome Black T, Rhodamine B. and Erythrosine decomposition, with the photocatalyst exhibiting better performance on Erythrosine. That was achieved due to dye molecules and photocatalyst surface (H^+ and $^{\bullet}OH$) electrostatic interactions. The NPs were prepared through sonication by a simple and rapid method with reagent the dithiooxamide, and various capping agents reporting that the different capping agents and fabrication affected the morphology of the samples. TEM images showed that the size of particle of $CuInS_2$ NPs is between 11 and 14 nm and a specific surface area of 11.96 m^2/g, while optical studies showed a bandgap of 1.53 eV making it convenient for photocatalytic application in the visible area as it showed photodegradation efficiency of 74.8 %.

Yang et al. [84], investigated the photocatalytic performance of two new 2D MSe_2 (M=Cd,Zn) structures for hydrogen production from water splitting using DFT calculations. Both structures were found to be thermally, kinetically and mechanically stable. $CdSe_2$ and $ZnSe_2$ sheets were found to have 2.13 and 2.26 eV band gaps, respectively, both structures in the visible and ultraviolet regions pronounced optical absorptions and have suitable band edge positions with respect to the water redox potentials. Moreover, it was studied the strain effect on both MSe_2 sheets electronic and optical properties in order to improve their photocatalytic performance while being promising for the water splitting photocatalytic reaction.

Politi et al. [85], investigated the influence of different precursors and ligands compositions on the synthesis of CdSe quantum dots via sonochemical synthesis. 625 different samples were composed using a workflow for material acceleration to reduce the chemical waste and experimental time for this study. The results showed that different ranges of composition of Se and Cd precursors only affected the particles generated number in contrast to the concentration of ligands that is controlling the particle size as cadmium ion's binding energy controls the nucleation synthesis rate. Approximately the particle size is within between 1.5 and 1.7 nm. It was also observed that the oleylamine presence favours the photoluminescence emissions while the addition of oleic acid not.

Zargarpour et al. [86], designed Fe-doped (0.25, 0.50, and 0.75 mM $FeCl_2$) and un-doped Cu_3Se_2 NPs via sonochemistry varying the concentration of Fe. Structural studies showed an uneven distribution of Fe atoms at the substantial and interstitial position. It was obtained that the Fe concentration increase prevents the formation of Cu_3Se_2 and that the addition of Fe didn't affect the samples morphology. Fe-doped samples were found to have an increase in NPs average size and varying the Fe concentration had an effect to the crystallite size ($\sim$8-44 nm). Moreover, the Cu composition in the samples was found to be low and can be attributed to the Cu-vacancy abundance in the crystalline lattice. The electrical and photocurrent properties of Fe-doped Cu_3Se_2 NPs was better and potentially can be used for novel and modern optoelectronic applications.

Matyszczak et al. [87], synthesised SnS and SnS_2 nano- and micropowders using sonochemistry varying synthesis conditions such as solvent, tin source ($SnCl_2$ or $SnCl_4$), thioacetamide molar ratio to the tin source and sonication time. It was observed that there is an influence of the used solvent on the sonochemistry as SnS_2 is mainly obtained by using methanol while SnS and SnS_2, and other compounds are obtained when the solvent is ethylenediamine. Moreover, characterisation studies revealed that the sulphide samples were almost homogeneous and the presence of Sn_2S_3 was reported. In addition, the synthesis conditions widely vary the morphology and the size from globular through flower-like to needle shape and from nano- to micro-powder, respectively, while longer sonication times increase the crystallinity and at the same time decrease the optical bandgap.

Un- and Zn-doped silver sulphide (Ag_2S) nanostructures prepared through sonication and parameters that affect its morphological, optical and structural properties were studied by Geravand and Jamali-Sheini [88]. The un-doped Ag_2S samples were prepared at three different sonication powers, 100, 200 and 300 W, with the greatest crystallite size (45 nm) refers to 200 W power application. It was obtained that the size of nanostructures decreases, and their optical bandgap energies change by increasing the sonication time and power. At 100, 200 and 300 W, the un-doped Ag_2S particles were grown all small, spherical and homogeneous with average diameters of 30.14, 23.53 and 27.16 nm. The Zn-doped Ag_2S

particles were synthesized through 15 min sonochemical process using 200 W power, using different concentrations of $ZnCl_2.4H_2O$. The crystallite size was shrined with the addition of Zn compared to that of un-doped Ag_2S, but is increased with the dopant's concentration from 18 to 36 nm. Lastly, the un-doped Ag_2S showed the most significant optical properties since the addition of Zn decreased samples optical bandgap.

4.3 Heterojunctions

The most widely used semiconductors for photocatalysis like Ti-based are known for possessing large bandgap and having a close spectral response range that cannot effectively absorb sunlight to realise the photocatalysis. The development of heterojunction was made to overcome this drawback of these semiconductors [89]. These materials compromise semiconductor and a radiation source combination that has enough energy to excite electrons in order to create a hole (h^+) in the valence band. The charge pairs react with different molecules to form reactive oxygen species [90]. The semiconductor heterojunction involves the stacking up to two semiconductors with different bandgaps. A heterostructure is blend of multiple heterojunctions where both designed forms can find application in lasers, transistors, photocatalysis, photodegradation of organic pollutants, solar cells and many more [91]. These materials can be obtained by several methods among them the sonochemical which is considered promising due to relatively simple apparatus use, short time of synthesis and no need for external heat source [90]. The sonochemical heterojunction construction has gained the interest of many scientists since the heterojunction surface can significantly improve charge carriers separation efficiency [92]. Table 1 presents the photocatalytic activity of different sonication assisted heterojunction photocatalysts.

Photocatalyst	Sonication conditions	Solvent	Materials	Type of heterojunction	Particle size (nm)	Photocatalytic activity	Ref.
$AgIO_4/TiO_2$	Ultrasonic bath for 3 h	Double distilled water (DDW),isopropanol (IPA)	Titanium isopropoxide, pluronic, silver nitrate, sodium metaperiodate, ammonia solution (NH_4OH) and methanol (MeOH)	Z-scheme	17-25	Photocatalytic hydrogen productio	93]
$Ag/\alpha\text{-}Fe_2O_3/TiO_2$	Pulse sonication at room temperature	Ethylene glycol (EG),deionized water (DI)	Titanium metal foil, ethanol (EtOH), acetone, NaF, $FeCl_3$ and $AgNO_3$	–	–	Photoelectrochemica water splitting	94]
$BiVO_3/g\text{-}C_3N_4$	Ultrasonic bath of 150 W for 2 h	EG	Urea, bismuth nitrate, sodium monovanadate, NH_4OH,EtOH, MeOH, amaranth dye, IPA, benzoquinone,ammonium oxalate and terephthalic acid	S-scheme	–	Hydrogen productio and degradation of amaranth dye	95]
$ZnCo_2O_4/Ag_3PO_4$	Ultrasonication	–	-	–	–	Degradation of methy orange and bispheno dye	96]
$BiVO_3/TiO_2$	Ultrasonic bath of 80 kHz for 2 h	EG	Titanium isopropoxide, triton-X-100, bismuth nitrate, sodium monovanadate,NH_4OH, EtOH, MeOH, rhodamine B dye, IPA, benzoquinone, ammonium oxalate and terephthalic acid	Z-scheme	–	Hydrogen productio and degradation of rhodamine B dye	97]

Table 1. (continued)

Bi_2WO_6/TiO_2	Probe sonicator with frequency of 20 kHz for 30 min	Nitric acid (HNO_3)	Degussa P25, glycerol, sodium tungstate dihydrate, potassium hydroxide, bismuth nitrate pentahydrate, NaOH and DI	Z-scheme	–	Photocatalytic hydrogen production	[98]
$Cu_2O@TiO_2$	Ultrasonic horn with frequency of 20 kHz for 15 min	DI and EG	Degussa P25 TiO_2, copper sulfate pentahydrate, ascorbic acid, poly(vinylpyrrolidone), sodium sulfate and methyl orange (MO)	–	–	Degradation of methyl orange	[99]
Ag_2O_3/CeO_2	Ultrasonic bath of 300 W	Distilled water (DW)	Ammonium cerium sulphate, MeOHl, silver nitrate, sodium carbonate and rhodamine B dye	Type (II)	–	Degradation of rhodamine B dye	[100]
$AgIO_4/CeO_2$	Ultrasonic bath of 200 W for 1 h, 50 °C	IPA, DW and DDW	Cerium nitrate, pluronic, silver nitrate, sodium metaperiodate, NH_4OH,EtOH, benzoquinone, ammonium oxalate and terephthalic acid	S-scheme	–	Degradation of rhodamine B dye	[101]
$ZnFe_2O_4/CeO_2$	Ultrasonication for 30 min, 75 °C	DI	Cerium nitrate, sodium hydroxide (NaOH), zinc nitrate hexahydrate,iron nitrate nonahydrate and NH_4OH	–	–	Degradation of malachite green	[102]

Abd-Rabboh et al. [97], synthesised a mesoporous $BiVO_4/TiO_2$ heterojunctions where the $BiVO_4$ NPs were incorporated on the surface of TiO_2 through sonochemistry by a certain ratio (2, 5, 10, and 15 w/w % $BiVO_4/TiO_2$). Nanoparticles such as $BiVO_4$ exhibit highly negative reduction potentials for the excited electrons and are suitable for coupling with wide bandgap semiconductors like TiO_2. The characterisation techniques showed the strong chemical interaction between the NPs. Also, it was investigated the ultrasound waves radiation power effect on rhodamine B (RhB) dye photodegradation and photocatalytic hydrogen production. Results showed the optimum value of 10 wt% for the $BiVO_4$ for RhB dye's photocatalytic degradation and hydrogen production and that the removal of RhB can be achieved under light radiations. The photostability of $BiVO_4/TiO_2$ after five consecutive cycles was found to be high for the decolourisation of RhB while the 80 % retains from its reactivity in the production of hydrogen. The charge carriers efficiency and the holes and electrons oxidizing and reducing power are enhanced by the Z-scheme mechanism.

Mahammed Shaheer et al. [98], investigated the synthesis of Bi_2WO_6/TiO_2 nanorod heterojunction by a sonochemical assisted impregnation method. It was obtained enhanced photocatalytic hydrogen production when compared to the performance of commercial P25 and TiO_2 nanorods. XPS analysis showed that ultrasonication promoted the metallic bismuth formation on TiO_2 nanorod and Bi_2WO_6 interface. The nanorod heterojunction showed visible light absorbance, excellent charge separation and transfer properties due to the TiO_2 1-D structure and the Z-scheme formation. The Z-scheme band was proposed based on the Mott-Schottky measurement, demonstrating efficient utilization of the Z-scheme heterojunction in photocatalytic reduction applications.

Cu_2O nanocube embedded on TiO_2 semiconductor via sonochemistry in order to synthesise a heterojunction nanocomposite was reported by Kaviyarasan et al [99]. Structure studies showed the cube-like structure formation of Cu_2O, while the presence of Cu, O and Ti elements oxidation states and the interaction between Cu_2O and TiO_2 were confirmed by XPS analysis. The heterojunction composite was assessed for its degradation ability of MO showing improved degradation when compared to pristine Cu_2O nanocubes and TiO_2 NPs. To find out MO's degradation pathway of that is following, HPLC chromatograph analysis was used showing that the intermediate demethylated methyl orange is formed (Figure 8). The photogenerated e^- from Cu_2O nanocubes are captured by P25 TiO_2 and get reduced from Ti^{4+} to Ti^{3+} ions. The holes in the Cu_2O valence band helps converting OH^- to $^{\bullet}OH$. Potentiostatic measurements took place in order to explain the Cu_2O nanocubes role on TiO_2, revealing their excellent photoelectric behaviour.

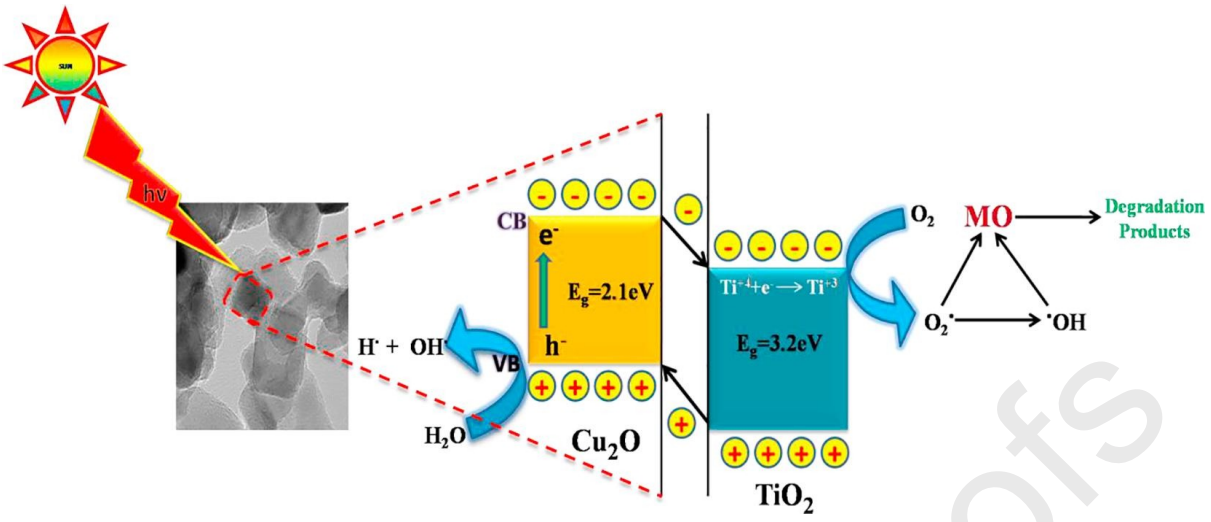

Figure 8. Mechanism of the photocatalytic degradation of MO catalysed by Cu_2O/TiO_2 heterojunction nanocomposite [99].

Heiba et al. [100], prepared an effective Ag_2CO_3/CeO_2-p-n heterojunction for the photocatalytic degradation of RhB dye under UV radiation. The heterojunction was formed through the sol-gel and sonochemistry techniques combination. Structural analysis showed the presence of large crystallite sizes of Ag_2CO_3 (150 nm) and the nanocrystalline size of CeO_2 of 7.4 nm. It was obtained that the lattice microstrain and crystallite size are not influenced by the composite (3 and 10%) of Ag_2CO_3/CeO_2 except the 5 wt% of Ag_2CO_3/CeO_2 where the microstrain is decreased and the size is increased. Moreover, experimental results revealed the positive role of Ag_2CO_3 in reducing the bandgap of CeO_2 from 2.9 to 2.7 eV. The toxic dye RhB photocatalytic degradation is a promising alternative to the traditional methods. Only 5% of RhB dye is decomposed in the absence of photocatalyst, while the optimum 5 wt% loading of Ag_2CO_3 on CeO_2 was found to be the most efficient with removal of 78 %. After 5 consecutive cycles the photocatalyst retained 80 % of its initial reactivity.

Alsalme et al. [101], investigated a synthesised novel $AgIO_4/CeO_2$ heterojunction constructed using ultrasonic bath of power of 200 W varying the composition of $AgIO_4$ (5, 10, 15 and 20 wt%). Characterisation techniques revealed a crystalline size reduction with increasing the $AgIO_4$concentration. Also, it is reported the high affinity of chemical interaction between $AgIO_4$ and CeO_2 NPs while experimental results indicating that the hybridization of the NPs generate step S-scheme heterojunction. The 15 wt% of $AgIO_4/CeO_2$ with a surface area of 49 m^2/g and crystalline size of 22 nm, was found to be the optimum composition for the decomposition of RhB with pseudo-first order rate of 0.024 min^{-1} which is higher than that of pristine CeO_2.

Ramasamy Raja et al. [102], prepared an eco-friendly photocatalyst, $ZnFe_2O_4/CeO_2$ at different molar ratios using sonochemistry. XRD patterns revealed the good crystallinity and the surface analysis showed the large surface area of the 0.5 $ZnFe_2O_4$:0.5 CeO_2 nanocomposite of 75.35 m^2/g which was larger than that of $ZnFe_2O_4$ and CeO_2. The average particle size was below 20 nm. The photodegradation, under visible light irradiation, of malachite green (MG) was examined using the 0.5 $ZnFe_2O_4$:0.5 CeO_2 resulting in a 96 % efficiency. The enhanced photocatalytic activity mechanism was illustrated proposing that the $ZnFe_2O_4$ is excited first by protons because of its narrow bandgap which led to the increased

electrons formation in its conduction and more holes in its valence band. The low bandgap of $ZnFe_2O_4/CeO_2$ was found to affect the degradation of MG dye and can be utilized as a visible light photocatalyst for wastewater treatment.

5. Reactors for Photocatalysis using Sonochemistry

5.1 Batch reactors

A large number of studies reported the sonication process or the photocatalytic experiments in batch systems [103]. Their set-up is simple and low-cost and therefore beneficial for different reactions. Batch reactors have been applied in different biological and chemical processes combined with ultrasound to escalate mass transfer phenomena and mixing. Nevertheless, is perplexed to scale and control, since the acoustic fields generated are non-uniform within conventional reactor systems [104], [105]. The majority of the research focuses on the photocatalytic experiments in batch configurations for the sono-synthesised catalysts instead of synthesising these materials in batch systems. Table 2 summarises different reactor configurations used for the sonochemical synthesis of photocatalysts and for the experiments.

Table 2. Types of reactors utilised for the experiments and/or synthesis of ultrasound-assisted photocatalysts.

Reactor	Photocatalyst	Sonication conditions	Solvent	Materials	Particle size (nm)	Target/Reaction	Efficiency	R
Batch	rGO-ZnS-TiO_2	240 W, 22 kHz	DW	Graphite powder, sodium nitrate, hydrochloric acid (HCl), concentrated sulphuric acid (H_2SO_4), hydrogen peroxide (H_2O_2), potassium permanganate ($KMnO_4$), NaOH, zinc chloride, IPA, titanium isopopoxide and sodium sulphide flakes	20-40	Crystal Violet (CV) dye	97%	[1
Batch	(rGO)-ZnO-TiO_2	-	DW, IPA	HCl, sodium nitrate, H_2SO_4, H_2O_2, $KMnO_4$, graphite powder, NaOH, titanium isopopoxide and sodium sulphide flakes	5-10	CV dye	87.06%	[1
Batch	ZnO	150 W	EtOH, DI	Zinc acetate, NaOH and EtOH	119-300	Hydrogen generation	n.d.	[1
Batch	Kronos 1077 TiO_2	50 W, 20 kHz	-	Isoproturon PESTANAL™,Kronos 1077, Degussa P25 nanometric TiO_2 catalyst, water and acetonitrile	-	Isoproturon (IPU)	>99 %	[1
Batch	P-doped TiO_2	-	EtOH, DI	Ciprofloxacin, phosphoric acid, tetrabutyl titanate, NaOH, HCl, IPA, potassium iodide and 1,4-benzoquinone	450	Ciprofloxacin (CIP)	90.63%	[1
Batch	GCN/MnO_2	250 W, 20 kHz	DI	Urea, HNO_3, $KMnO_4$ and polyethylene glycol (PEG)	190.5-210.3	Tetracyline hydrochloride (TcH)	93%	[1
Batch	CuO NPs	400 W,	DW	Copper (II) sulfate, Cystoseira trinodis, DDW, and DI	6	Methylene Blue (MB) dye	98%	[1
Continuous flow	TiO_2	150 W, 37 kHz	EtOH, DI	Titanium Tetraisopropoxide, lactic acid and citric acid	50-160	Pollutant gas (NO)	n.d.	[1
Continuous flow	CuO/CuO_2/Cu	200 W,	DI	Copper acetate monohydrate,ammonia and DW	_	Safranin O (SO) dye	98.10%	[114]

Table 2. (continued)

Continuous flow	$CuO/CuO_2/Cu$	200 W, 50-60 kHz	DI	Copper acetate monohydrate,ammonia and DW	_	MB dye	91.91%	[114
Continuous flow	Ag[Cu@Ag]/APTMS/boehmite	_	DI	Aluminum nitrate nonahydrate NaOH, HCl, methylene blue, calcium chloride, cupric sulfate, tri-sodium citrate dehydrate, sodium borohydride, sodium alginate, (3-aminopropyl) trimethoxysilane and silver nitrate	45-50	MB dye	80.3 % (visible light)	[115
Continuous flow	Ag[Cu@Ag]/APTMS/boehmite	_	DI	Aluminum nitrate nonahydrate NaOH, HCl, methylene blue, calcium chloride, cupric sulfate, tri-sodium citrate dehydrate, sodium borohydride, sodium alginate, (3-aminopropyl) trimethoxysilane and silver nitrate	45-50	MB dye	40.7 % (light irradiation)	[115
Continuous flow	$Bi_2MoO_6/FeVO_4$	50 W, 40 kHz	EG and DI	Iron (III) nitrate nonahydrate, bismuth nitrate pentahydrate, ciprofloxacin H_2O_2,anhydrous EtOH, ammonium metavanadate,sodium molybdate dihydrate	_	CIP	91%	[116
Continuous flow	Ag_3PO_4/Bi_2S_3-HKUST-1-MOF	25 kHz	DDW	NaOH, HCl, silver nitrate, di-sodium hydrogen phosphate, sodium sulfide, bismuth (III) nitrate penta hydrate, hydrated copper nitrate, trypan blue and vesuvine	_	TB	98.44	[117
Continuous flow	Ag_3PO_4/Bi_2S_3-HKUST-1-MOF	25 kHz	DDW	NaOH, HCl, silver nitrate, di-sodium hydrogen phosphate, sodium sulfide, bismuth (III) nitrate penta hydrate, hydrated copper nitrate, trypan blue and vesuvine	_	Vesuvine (VS)	99.36%	[117
Continuous flow	CdS nanoplates	100 W	_	Cadmium chloride, thiourea, ammonium chloride–ammonium hydroxide buffer	20-0.5 (μm)	_	_	[118
Continuous flow	Pt/graphene	_	DW	H_2SO_4, graphite, $KMnO_4$, H_2O_2, HCl, NaOH, hexachloroplatinic acid and EtOH	1.75	_	_	[119
Continuous flow	Pt/TiO_2	_	DW, EtOH	Titanium dioxide (TiO_2) and hexachloroplatinic acid aqueous solution	3.77	_	_	[119]

Table 2. (continued)

Continuous flow	Au/TiO_2	_	DW, EtOH	TiO_2 and hydrogen tetrachloroaurate(III)	3.8	_	_	119]
Mesoscale	TiO_2	20 kHz, 31.4 °C	Acetonitile	TiO_2, anatase, (trifluoromethyl)benzyl alcohol and acetonitrile	3.8 (μm)	4-(trifluoromethyl) benzyl alcohol	86%	120]
Mesoscale	TiO_2-ZnO	1000 W, 22 kHz	DW	Titanyl sulphate, zinc nitrate hexahydrate	_	Acid Orange 7 dye	3.63%	121]
Mesoscale	TiO_2	1000 W, 25 kHz	_	Phenol crystals, H_2O_2) and TiO_2 (mixture of anatase and rutile forms)	_	Phenol	37.75%	122]
Microscale continuous flow	TiO_2	_	Milli Q	Commercial TiO_2 (Aeroxide® P25) and phenol	_	Phenol	11% (visible light)	123]
Microscale continuous flow	Bi_2O_3	_	HNO_3	Bismuth(III) nitrate pentahydrate, HNO_3, NaOH, polyvinyl-pyridine (PVP), triethanolamine, IPA, MO, Poly(dimethylsiloxane) (PDMS) and curing agent (Sylgard 184 silicone elastomer)	6.7	Methyl orange (MO)	96%	124]
Microscale continuous flow	ZnO	16 W	_	_	_	Benzyl alcohol	_	125]
Microscale continuous flow	$Ag/g\text{-}C_3N_4$	60 W	DI	Melamine, silver nitrate, H_2SO_4, sodium borohydride and triethanolamine	3-8	Water splitting for H_2 generation	_	126]
Microscale continuous flow	LFO/PU	_	DW	Tetracycline, Lanthanum nitrate hexahydrate, iron (III) chloride, calcium chloride, ethylene diamine tetra acetic acid disodium salt, IPA, benzoquinone, HCl, NaOH, citric acid, urea, NH_4OH, H_2O_2 and EtOH	_	Tetracyline (TC)	94%	127]
Microscale continuous flow	CFO/PU	_	DW	Tetracycline, Lanthanum nitrate hexahydrate, iron (III) chloride, calcium chloride, ethylene diamine tetra acetic acid disodium salt, IPA, benzoquinone, HCl, NaOH, citric acid, urea, NH_4OH, H_2O_2 and EtOH	_	Tetracyline (TC)	80%	127]
Microscale continuous flow	TiO_2	120 W, 37 kHz	IPA	Titanium (IV) Isopropoxide, TiO_2 (P25), benzyl alcohol, EtOH, MeOH, acetonitrile and phosphoric acid	<35	Benzyl alcohol	6%	[128]

Multifunctional rGO-ZnS-TiO_2 photocatalytic NPs were prepared through sonochemistry for crystal violet's (CV) dye removal from wastewater. Kale et al. [106], synthesised the nanocomposites with a conventional method and under ultrasound of 240 W power and 22 kHz. The size of TiO_2 particles synthesised by the conventional method was around 70-80 nm while via ultrasonic method was 20-40 nm. The successful formation of the NPs was validated by various characterisation techniques and tested them for their photocatalytic degradation in a batch reactor (volume = 100 mL). A superior photocatalytic performance was observed as approximately 97 % of CV dye was successfully removed by adsorption making this photocatalyst suitable for the CV dye photocatalytic degradation.

Another study for the photocatalytic CV dye degradation was investigated by Potle et al [107]. A conventional and a sonochemical method were used for the design of ternary (rGO)-ZnO-TiO_2. Characterisation analysis showed the evenly dispersion of ZnO and TiO_2 particles on the graphene sheet with the utilisation of ultrasound with a small particle size of 5-10 nm. The CV dye photocatalytic degradation took place in a 100 mL batch reactor and the initial concentration of the dye was 50 ppm. The (rGO)-ZnO-TiO_2 photocatalyst synthesised by ultrasound showed around 15% higher photocatalytic degradation than the material prepared by the conventional technique under the same experimental conditions.

Luévano-Hipólito et al. [108] synthesised a ZnO photocatalyst via a sonochemical method for hydrogen generation via a heterogeneous photocatalysis. A sol-gel method was used, and the mixture was exposed to ultrasound irradiation (150 W) and a temperature of 70 ^oC. When the mixture was exposed to ultrasonic waves the basic medium promoted the generation of radicals as $^{\bullet}H$ and $^{\bullet}OH$ was reported. The photocatalytic reaction took place in a cylindrical Pyrex batch reactor. The experiments showed that the ZnO samples photocatalytic activity was affected by various parameters and major influence was attributed to small particle size (119-300 nm) and high surface area (20-38 m^2/g). Moreover, it was observed that when the ratio of (0 0 2) and (1 0 0) planes was higher than 1, a low photocatalytic activity was achieved. XRD and HRTEM analysis confirmed that when (1 0 0) crystal planes are present in high amounts ZnO catalyst exhibits high H_2 production while low amount of (0 0 2) planes relate to a higher amount of oxygen vacancies that decrease the activity of the photocatalyst due to photocorrosion phenomenon. The highest H_2 generation achieved was 107 $\mu mol\ g^{-1}\ h^{-1}$.

The photocatalytic degradation of the Isoproturon (IPU) herbicite was tested by Schieppati et al [109]. Kronos 1077 was utilised as micrometric TiO_2 catalyst was tested and compared with the P25 nanometric TiO_2 catalyst. Sonolytic and photocatalytic tests ran separately and then were combined into one technique (sono-photocatalytic method) with an ultrasonic power of 50 W and a frequency of 20 kHz. A batch thermostatic glass reactor was used for all the tests with a constant temperature of 15 ^oC. A 0.1 g/L catalyst amount resulted in a complete degradation of the IPU, with an initial concentration of 20 ppm, in 1 h by the sonophotocatalysis method. Both photocatalysts were active and therefore Kronos 1077 can replace the P25 catalyst since the later arises some serious health and environmental concerns. Moreover, ultrasound-assisted photocatalysis lead to by-products with lower molecular weight when compared to photocatalysis single method.

The effect of hydrodynamic cavitation (HC) and photocatalytic techniques was investigated by Chen et al. [110] for organic contaminants removal. P-doped TiO_2 photocatalysts were synthesised for the degradation of ciprofloxacin (CIP) varying the molar ratios of P/Ti (0.02, 0.04 and 0.06). Optimal experimental conditions and the synergistic effect of HC and photocatalytic processes reached a high CIP degradation as high as 90.63 % in a photocatalytic batch reactor. The observed results were an effect of the smaller particle size (~450 nm), increased and cleaner surface area (144.3 m^2/g for P-TiO_2-0.04) and lastly improved dispersion that were confirmed by SEM, TEM, and BET analysis. The author concluded that this efficient HC-assisted photocatalytic process has future potential for the treatment of pollutants at the industrial scale.

Photocatalytic investigations for the degradation of tetracyline hydrochloride (TcH), a toxic pharmaceutical compound was studied by Yashas et al [111]. Nanocomposites of GCN/MnO_2 were designed by a sonochemical method (250 W, 20 kHz) with different mass of GCN (50, 100, 200 mg named CMn_1, CMn_2 and CMn_3 respectively). Characterisation techniques revealed that morphology, crystallinity, and other material properties were modified by ultrasound application. The obtained particle size was 190.5, 195.2 and 210.3 nm for the CMn_1, CMn_2 and CMn_3 catalysts. The photocatalytic degradation of TcH was tested in quartz beakers of 100 mL volume (batch mode). Approximately 93% degradation was achieved in 135 min and with 30 mg catalyst amount. Additionally, a reusability study was conducted where after four cycles, an 11% decrease in the photocatalytic degradation was observed.

CuO NPs were biosynthesised by an ultrasound method (400 W, 20 kHz) utilising the Cystoseira trinodis extract for both time-saving and as an eco-friendly approach by Gu et al [112]. A spherical crystallite structure with a size range of 6-7.8 nm was observed by SEM analysis. Photocatalytic studies were performed in a batch reactor (150 x 75 mm) for the evaluation of the performance of the photocatalysts. 5 ppm of Methylene Blue (MB) were loaded in the reactor along with the CuO NPs and were exposed to visible and UV light. Under UV light and pH 4, the photocatalytic degradation of MB reached up to 98%. The synthesised photocatalysts were tested for antibacterial activity and for the inhibition of the activity of DPPH free radicals with exceptional results.

Most of the times a medium size beaker is used as a batch reactor in photocatalytic experiments, mainly due to their easy set up and operation. Nevertheless, conventional configurations are not utilised for the sono-synthesis as they do not significantly affect the synthesis of NPs due to the simplicity of the system. As far as it concerns the photocatalytic experiments the simplicity of the system allows the technique to give satisfactory results.

5.2 Continuous flow reactors

Even though the utilisation of batch reactor to evaluate the photocatalytic performance various NPs is beneficial, continuous reactors seem to improve the irradiation when the reaction mixture is exposed to. When it comes to continuous flow reactors the time of reaction time is decreased, achieving higher production rates and enhanced yield when compared to batch systems. Continuous flow systems are also utilised for the synthesis, generating particles with narrow size distribution, enhanced uniformity and with several effects on the morphology such as crystallinity and porosity which cannot be achieved in a batch reactor. If the process allows, is preferred to use continuous reactors instead of batch since they meet industrial production demands [105].

The synthesis of TiO_2 using no acid, lactic acid and citric acid in a sonochemical process for the production of samples with different morphologies regarding crystalline phase and particle size was conducted by Palacio et al. [113]. The formed samples (S1, S2 and S3) were subjected for 1 h to sonication at 150 W and 37 kHz. The particle size was 137±28, 65±14 and 73±18 nm for S1, S2 and S3 respectively. Colorimetric method was used to evaluate their photocatalytic performance where the samples were irradiated by LEDs, measuring the change of colour. The evaluation of their photocatalytic capacity, a continuous flow photoreactor was utilised with a constant flow of pollutant gas (NO) following the established guidelines by ISO 22197-1. A dynamic calibrator and a bubble humidifier were utilised for the continuous gas flow supply with the reactor diagram shown in Figure 9. The initial gas concentration and the change over time were measured when the samples were exposed to UV light cycles. All three samples achieved good photocatalytic performance even though the TiO_2 particle size was larger with the absence of organic acid during synthesis.

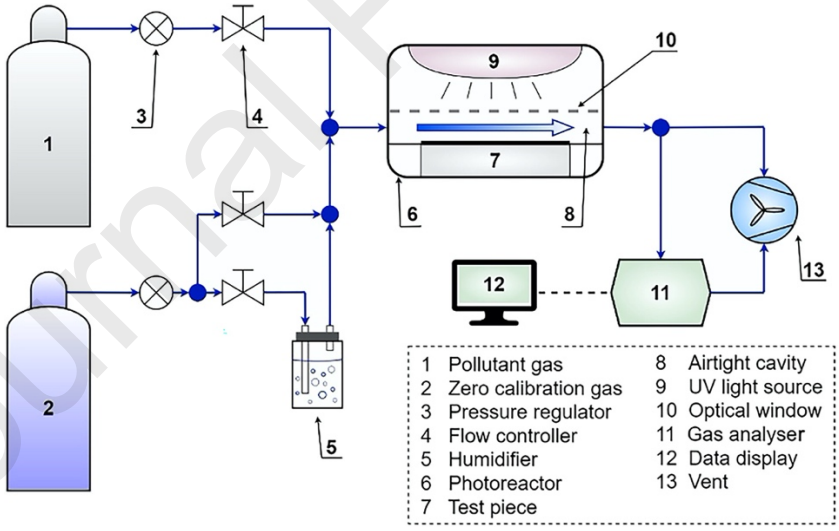

Figure 9. Illustrative diagram of the continuous flow photocatalytic reactor [113] .

Mosleh et al. [114] synthesised $CuO/CuO_2/Cu$ NPs through the combination of sonochemical and thermal methods where it was then utilized as a photocatalyst for safranin O (SO) and

MB dyes degradation in a novel rotating packed bed reactor equipped with a blue LED instead of UV lamps. It was found that the high centrifugal field of the reactor is advantageous for the interfacial surface area caused by the rotational speed which enhances the mass transfer and mixing process. Central composite design (CCD) was used in order to obtain the optimum photocatalytic degradation of SO and MB dyes. The results showed great photocatalytic performance with 98.1% and 91.91% photodegradation percentage for SO and MB dyes, respectively.

Miri and Ghorbani [115] investigated the degradation of an ultrasonic photocatalyst in batch and continuous flow reactors under visible light. For the synthesis of nano-boehmite of Ag[Cu@Ag]/APTMS/boehmite nanocomposite photocatalyst, an ultrasonic bath was used for 3 h at 25 ^{o}C. The resulted photocatalyst had a mean size of 45-50 nm and increased surface area of 603 m^2/g. The photocatalytic MB dye degradation was studied in a batch reactor with constant temperature at 25 ^{o}C maintained by a cooling system. Additionally, a continuous reactor was utilised to perform the degradation reaction. The reactor was fixed on a mirror for the enhancement of the light irradiation and was packed with glass beads, covered by alginate- Ag[Cu@Ag]/APTMS\boehmite. The removal rate of the dye, in the optimum condition, under the visible light using the photocatalyst, in the batch reactor was 80.3% within a period of 47 h while under the solar light, for over 8 h, the removal rate was 40.7%. The continuous flow reactor was used as an industrial system model and was studied considering the initial concentration of dye and flow rate as variables. It was obtained that the decrease of both variables increased the degradation rate of the dye.

Fan et al. [116] designed a suspension sono-photocatalytic membrane reactor (SPMR) for the stable and continuous ciprofloxacin (CIP) degradation by $Bi_2MoO_6/FeVO_4$ sono-photocatalyst. The continuous SPMR was composed with the ultrasonic generator of 40 kHz frequency and 50 W power, while the hollow fiber membrane was used to retain and stabilise the catalyst and the catalyst concentration in the reactor. The crystallite size was 7.2±3 nm and surface area 56.28 m^2/g. Combining sonocatalysis and photocatalysis was found to improve the CIP degradation with synergy index of 1.80. The analysis of the membrane before and after the use in the SPMR system reporting that the membrane played a role in the CIP degradation. Moreover, experiments took place to assess the stability of the continuous SPMR indicating that the presence of membrane, ultrasound, light and the addition of a strong oxidizing agent (H_2O_2) improved the CIP removal. After one hour the reactor was found to reach steady state demonstrating the continuous and stable operation potential. The optimum hydraulic reaction time (HRT) was 720 min with removal of CIP of around 91 %.

Mosleh et al. [117] used a continuous flow-loop reactor for the TB and vesuvine (VS) sono-photocatalytic degradation utilising the novel Ag_3PO_4/Bi_2S_3-HKUST-1-MOF photocatalyst synthesised by sonochemical assisted solvothermal method. The reactor set-up that includes the reactor vessel and the ultrasonic bath is shown in Figure 10. A CCD investigation for the effect of operational parameters such as dyes concentration, flow rate, irradiation and sonication time were occurred. At the optimum conditions of 25 mg/L of each dye, flow rate of 70 mL/min, 25 min of irradiation and sonication time, pH 6.0 and photocatalyst dosage of 0.25 g/L, the maximum sonophotodegradation percentage of TB and VS dyes was 98.44 and 99.36 %, respectively. Moreover, a synergistic value of 2.53 was obtained, indicating that the combination of ultrasound irradiation and photocatalysis have higher efficiency than the individual processes.

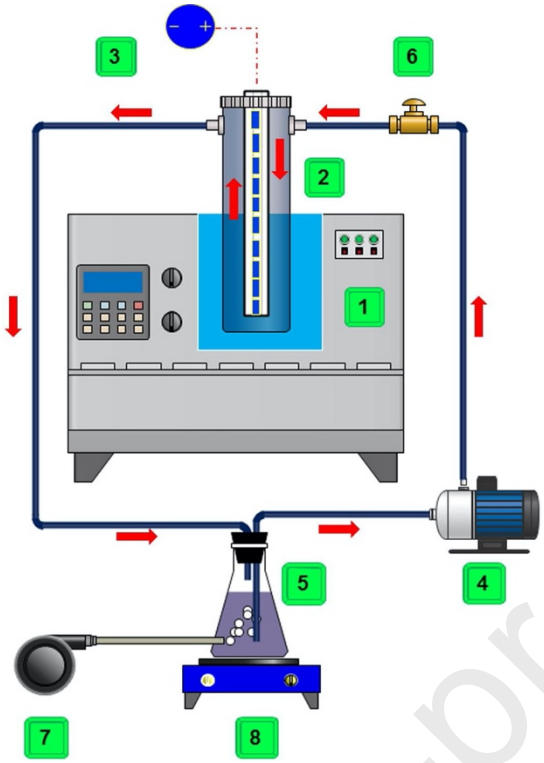

Figure 10. Sonophotocatalytic reactor set-up: (1) ultrasonic bath, (2) reactor vessel, (3) LED source, (4 peristaltic pump, (5) reservoir, (6) sampling pump, (7) aeration pump and (8) magnet pump) [117] .

Continuous flow reactors can be utilised in the synthesis of sonicated photocatalysts for industrial purposes as batch reactors are difficult to scale-up. Palanisamy et al. [118] developed a continuous flow sonochemical reactor for the continuous production of CdS nanoplatelets with thicknesses not exceeding 10 nm with a particle size ranging from 20 to 0.5 µm after 1 h of synthesis. The synthesised nanoplatelets were compared to those from batch reactors including conventional heating and ultrasound assisted heating. It was observed that continuous flow synthesis is capable of producing a metastable phase of CdS where cubic platelets were mainly generated. In contrast, in batch ultrasound assisted reactor a mixture of cubic and hexagonal platelets was obtained while in the conventional heating batch only hexagonal platelets were present. Also, it was reported that is much faster the continuous sonochemical synthesis where it can be attributed to the well mixing of reagents and the thickness of nanoplatelets indicates their application as quantum wells.

Abdolhosseinzadeh et al. [119] used for the metallic NPs controlled deposition, a continuous flow reactor. The reactor consisted by a PVC pipe (15 x 55 cm) and quartz tubes inside (0.5 x 55 cm) covered with adhesive-backed aluminum foil, sampling tubes, evacuation valves and a syringe. Different composite systems were prepared (Pt/graphene, Pt/TiO_2 and Au/TiO_2), with the suspension being sonicated by a probe sonicator, resulting a 1.75, 3.77 and 3.8 nm particle size, respectively. It was observed that cations reduction was complete and efficient, and the amount, location, and deposition rate were controllable indicating that the synthesis method of the NPs using the continuous flow reactor was successful. Moreover, it was observed that the illumination dose per exposure (IDE) should be optimised for each nanoparticle in order to get the best product quality at the highest yield. The results clearly show the potential and ability of the reactor for the continuous production of nanoparticle catalysts on large scale.

Continuous flow reactors can be utilised either to perform photocatalytic experiments to study the activity of different photocatalysts produced by sonochemistry by the degradation of dyes or to synthesise sonicated photocatalysts. The implementation of continuous flow reactors in the production of photocatalysts is showing their potential application in large scale as the synthesis is faster than in a batch reactor.

5.1.1 Mesoscale reactors

Lab-scale reactors are essential for experiments but their scale-up is mandatory to achieve industrial level. Meso-scale or pilot scale reactors are usually up-scaled bench systems as middle point to transfer into a full commercial unit.

A continuous-flow meso-scale ultrasonic reactor of 12.88 mL volume was used to perform photochemical transformations by Dong et al [120]. The purpose of this work was the development of an ultrasonic reactor that can handle the clogging of the reaction channels. The set-up of the reactor consists of a mass flow controller, a syringe pump, an illuminating box with UV LED light and a signal detector. The aerobic oxidation of 4-(trifluoromethyl) benzyl alcohol was carried out by the TiO_2 catalysts presence. The generation of cavitation bubbles by the ultrasound irradiation (frequency of 20 kHz) can improve the mixing, allowing the precipitated particles resuspension within 2 s and break-up of the agglomerated particles. Thus, the photon absorption is enhanced resulting in a positive effect of benzyl alcohol transformation to benzaldehyde.

Textile coated with TiO_2, ZnO and combination of both were synthesised for the comparison of their antibacterial properties by Abramova et al [121]. A laboratory setup was used for the sol-gel methods to synthesise the NPs through an ultrasonic acoustic field where the maximum power was 1000 W and 22 kHz of operating frequency. The second part of the study utilised a semi-industrial roll to roll machine to test the possibility of scaling up the proposed method as shown in the figure below (Figure 11). The setups were also used for the investigation of the photocatalytic properties. Acid Orange 7 dye was used for photodegradation whereas the photocatalytic activity of the coating was confirmed. Antibacterial efficiency of the fabrics was studied using Escherichia coli. Stable antibacterial properties were achieved with 99.99% suspension level of E.coli.

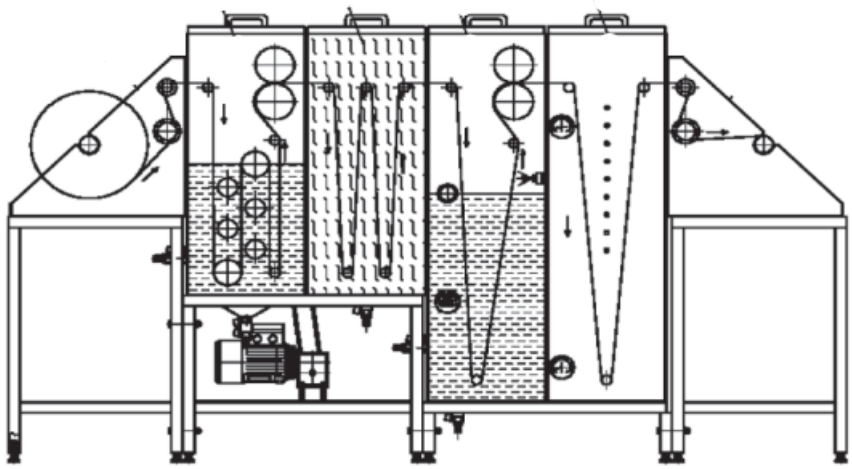

Figure 11. Schematic diagram of the roll to roll coating machine [121].

A pilot-scale sonochemical reactor configuration was developed for the degradation of phenol with different treatment methods by Khokhawala and Gogate [122]. UV irradiation and ultrasound were tested separately. The reactor utilised was basically an ultrasonic bath with a transducer of power output of 1000 W and frequency of 25 kHz. For the experiments involving the solid catalyst (TiO_2), a six-blade turbine agitator (480-500 rpm) was used for the uniform suspension of the NPs. For the individual experiments, 90 min were enough for the phenol degradation while for the combination of the two techniques the experiment was performed for 180 min for the validation of the synergistic effect. Photolysis exhibited higher efficiency than ultrasonic treatment but when the two modes were combined the efficacy achieved was even higher. Sonophotocatalysis assisted by adding of 1% H_2O_2 exhibited the best degradation of phenol (37.75%). The authors through the synergistic effect of the two methods in a pilot-scale reactor concluded that is promising for the scale up in industrial level for either a pre-treatment strategy for wastewater or for the removal of contaminants.

Meso-scale reactors are used as scaled up systems to finally achieve industrial level. In the case of photodegradation of sono-synthesised catalytic NPs, pilot-scale are usually continuous flow systems since they offer great advantages compared to conventional reactors.

5.1.2 Microreactors

Microfluidics offers several advantages over bulk chemistry, one of which is slow diffusion. Consequently, to accelerate reactions, it is necessary to decrease the distance required for interaction. The reduced dimensions of microchannels also aid in minimising the sample volume needed for analysis, thereby reducing by-products. Recent advancements in this field have highlighted the benefits of reactor miniaturisation in terms of kinetics, safety, and cost efficiency. The synthesis of NPs using microfluidics has gained prominence in recent year [129]. Improved irradiation is achieved by the adoption of continuous flow microreactors within the reaction mixture, resulting in significantly reduced reaction times and improved product yields compared to batch reactors [130]. Batch reactors suffer from the drawback of a linear decrease in electromagnetic radiation intensity with the square of the distance from the light source. Photocatalytic microreactors overcome this limitation by providing homogeneous irradiation across the entire microchannel surface when exposed to the light source [131]–[133]. Additionally, by controlling the injection flow, molecules undergoing photodegradation constantly exit the reaction environment, preventing the accumulation of by-products in the reaction mixture.

Carlos Colmenares et al. [123], proposed a novel ultrasound-assisted method for the TiO_2 photocatalytic NPs deposition on the inner walls of microchannels. Changes in the inner surface of the FEP microtubes were observed after the ultrasonication process such as etched surface and rough spots, creating an environment for stable immobilisation for the TiO_2 NPs. The removal of phenol in water was utilised to test the TiO_2 coated FEP microtubes photocatalytic performance. The flow in the microchannel was constant at 0.05 mL/min and the photocatalyst was exposed at UV light of 125 W for 60 minutes. The results from the photocatalytic degradation were analysed using an HPLC where the different samples tested showed the degradation of phenol (TOF = 0.41 s^{-1}). The photocatalytic phenol degradation was tested under visible light and UV light conditions resulting in 11% and 41% degradation, respectively. Batch photoreactor experiments were also studied for comparison purposes giving lower grade of phenol degradation with a TOF value of 0.03 s^{-1}.

Katoch et al. [124], utilised a microreactor for both flow synthesis and photocatalytic experiments of Bi_2O_3 NPs with narrow particle size distribution. Syringes with the precursors were loaded in a T-shaped microreactor (Figure 12) with a diameter of 450 μm, through a microfluidic pump with 100 μL/min flow rate and spherical Bi_2O_3 (~6.7 nm) particles with ~6.7 nm particle size and 17.967 m^2/g surface area were obtained. To evaluate the Bi_2O_3 NPs photocatalytic performance, methyl orange (MO) degradation was studied in a conventional (beaker) method and in a microreactor. Firstly, the photocatalysts were deposited in the inner walls of the microreactor using a sonication-based dispersion technique and then the reactor was placed under visible light of 100 W, followed by the injection of MO at 50, 100, and 200 μL/min. For the conventional method a degradation of 76% was achieved after 225 minutes, while with the microflow reactor 96% of the dye was degraded by visible light in 15 minutes. Flow rate increase, results in photocatalytic performance-declined, and therefore it is evident that the optimum flow rate is 50 μL/min. Moreover, great photostability was demonstrated after three cycles. Further studies showed that Bi_2O_3 photocatalytic NPs prepared by microfluidics present an excellent antibacterial activity even at low concentrations for the inhibition of E.coli pathogen.

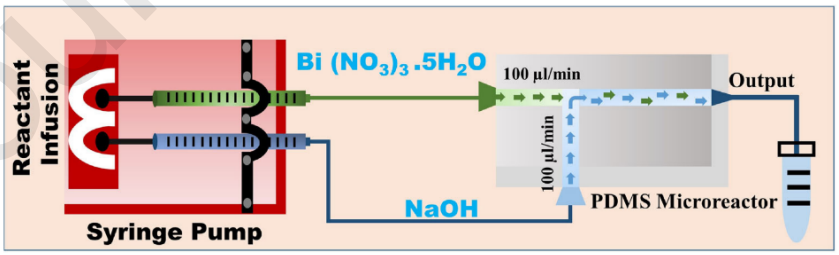

Figure 12. Schematic diagram of the microfluidic setup used the synthesis of Bi_2O_3 NPs [124].

Added value chemicals from biomass were produced using a commercial ZnO NPs deposited along the inner walls of a fluoropolymer (FEP) photo-microreactor by Nair et al [125]. The deposition took place utilising different flow rates and ultrasound powers of the ultrasound bath at mild temperature conditions. For the evaluation of the ZnO tubes, photocatalytic experiments were took place in batch and microflow photoreactor for the benzyl alcohol oxidation to benzaldehyde using a UV-LED light source with a power of 16 W. The flow of the benzyl alcohol in the microreactor was constant (0.053 mL/min) and introduced in the reactor by a syringe infusion pump. The ZnO photostability in a single coated FEP channel was tested in five continuous cycles showing a slight decrease in the catalytic activity. The experiments were carried out for six hours and the highest conversion (1.8 mol/m^2.h)) and selectivity (98%) were achieved after 15 min of reaction in acetonitrile (ACN) solvent. When the solvent was milli-Q water, the conversion rate was 288 mol/m^2.h and the selectivity 14.6 %. The conversion and selectivity in the photocatalytic batch reactor were much lower (0.07 mol/m^2.h and 23.7% for ACN and 0.6 mol/m^2.h and 20.5% for water), highlight the significance of the reactor utilised for the experiments.

A coiled flow inverter microreactor (CFIR) was utilised by Zhu et al. [126] for the synthesis of Ag/g-C_3N_4 photocatalysts with controllable sizes (Figure 13). The CFIR consisted of tubes with 0.03-inch inner diameter, 1/16-inch outer diameter and a 3-D printed framework with precise geometric parameters such as helix diameter, pitch distance and channel length. The prepared mixture was introduced to the reactor by syringe pumps with a constant 2 mL/min flow rate. The ultrasound and residence time effect was investigated and with increasing the output power (0 W - 120 W) and residence time decrease from 140 s to 17.5 s, the silver NPs size decreases with a narrower distribution. High catalytic activity was observed under 60 W that was 1.22 times higher than the catalyst's activity prepared without ultrasound. Higher Ag loading was also tested (7 wt. % Ag/g-C_3N_4) exhibiting an even better catalytic performance approximately 3 times higher than pure Ag/g-C_3N_4 for 35 s.

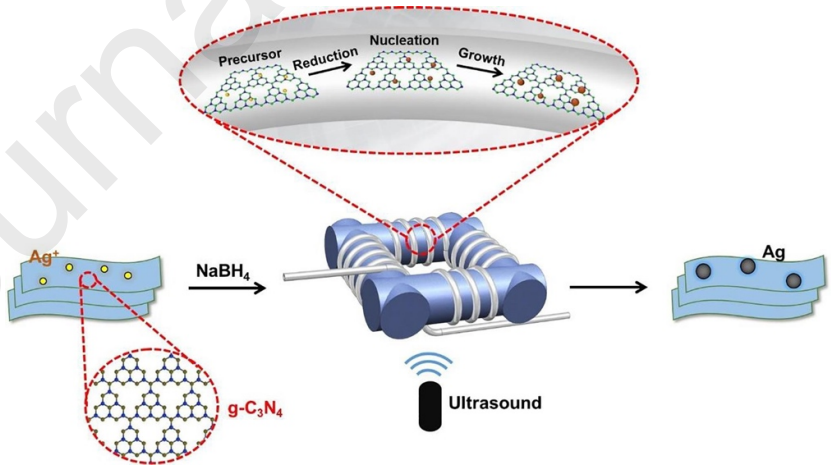

Figure 13. Schematic diagram of the experimental set-up [126].

$LaFeO_3$ and $CaFe_2O_4$ highly efficient perovskites were deposited in polyurethane filters (LFO/PU, CFO/PU) with the assistance of hydrotreatment and ultrasound by Tuna et al [127]. SEM analysis showed that raw CFO and LFO samples had a multilayered structure composed by spherical particles. After the deposition on the Pu filters both particles were

homogeneously dispersed and the structure changed into irregularly shaped particles, denoting that the sonication step affects the synthesised particles size. In a micro-column reactor, continuous flow photo-Fenton experiments took place for the photodegradation of tetracyline (TC) (Figure 14). The microreactor had an internal dimension of 1.25 cm and length of 6 cm where the catalytic filter was placed. The effect of TC inlet concentration was investigated using three different concentrations (5, 10, 15 mg/L). The optimum performance was for the 5 mg/L TC initial concentration where after 7 h the removal percentage was 44% and 83% for the CFO/PU and LFO/PU respectively. High TC concentrations may block the active sites of the catalytic material with antibiotic molecules that obstruct light absorption. Different flow rates were also studied (0.17, 0.3, and 0.6 mL/min) and it was observed that lower flow rates result in a higher rate of antibiotic removal since contact time is increased. For CFO/PU and LFO/PU the removal efficiencies were 37% and 53% respectively. The authors concluded that both samples could be long-lasting photocatalysts for the application of continuous visible light driven processes.

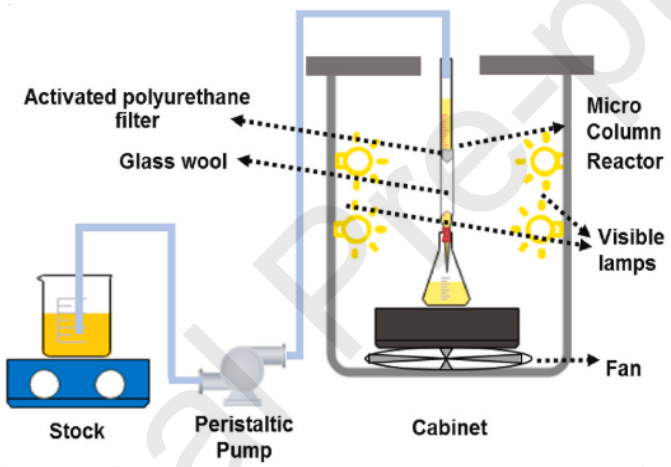

Figure 14. Diagram of the set-up of the micro column reactor [127].

Pradhan et al. [128], investigated the ultrasound-assisted synthesis and deposition of TiO_2 NPs for the photocatalytic performance of the oxidation of benzyl alcohol in continuous flow. The preparation of the photocatalysts was conducted by the sol-gel based method followed by sonication for 1 h with 37 KHz and 100% power. The deposition of the TiO_2 particles on the inner walls of a perfluoroalkoxyalkane (PFA) microreactor took place in mild conditions using ultrasound irradiation (120 W, 37 kHz). The synthesised catalyst had particle size less than 35 nm and high surface area of 284 m^2/g. For the photocatalytic studies, a batch system was first utilised to optimise key parameters such as loading of catalyst, solvents and stirring rate to determine the best experimental parameters for the continuous flow tests. It was observed that continuous microflow reactors (0.134 mL/min of benzyl alcohol) resulted in improved benzyl alcohol conversion and benzyl aldehyde selectivity and shorter reaction times. Commercial catalysts were also tested and compared with the sol-gel synthesised

catalysts where their main difference was that the later had five times higher specific surface area. In microflow reactor TiO_2-SG photocatalysts exhibited better results since with the deposition there are more available active sites on the channel's walls but in the batch system P25 commercial catalyst had a higher oxidative conversion performance.

Ultrasonic microflow reactors have been applied for the synthesis and deposition of photocatalytic materials. Their characteristic micro-size channel acts in favour of controlling mass/ heat transfer and reaction conditions, offering similar advantages of commercial-scale reactors. Therefore, continuous flow microreactors are preferred from batch systems.

6. Conclusions

Considering the effects on the climate from the global environmental crisis, green chemistry is a developed field that aims to achieve sustainability in the synthesis of materials and also the reduction of hazardous substances. Sonochemistry can be utilised to synthesise nanomaterials with the application of ultrasound waves offering a control on the crystallinity of the materials. The ultrasound assisted synthesis of photocatalysts finds application in many sectors such as the decomposition of hazardous and toxic substances and the removal of dyes. The acoustic wave synthesis of metal nanoparticles can be utilised for metal oxides synthesis, metal chalcogenides and heterojunctions. The incorporation of sonochemistry on the materials synthesis improved their crystallinity, lowered the particle size, and increased the catalyst surface area. The ultrasound synthesis of photocatalyst and their photocatalytic reactions are mainly performed in batch reactor systems due to the simplicity of the system and low-cost. Moreover, continuous flow reactors not only can obtain higher yields in photocatalytic processes, operate faster than the batch reactors but also to be utilised in large scale processes. In addition, the advantages offered by microfluidic reactors focus mainly in the advanced photocatalytic reactions efficiency and in the reduction of reaction time compared to batch systems.

Acknowledgments

We would like to thank Erasmus + for the opportunity to be a part of the research team in the University of Milan, Department of Chemistry.

Conflict of Interest

The authors declare that they have no known competing financial interests or personal relationships that could have appeared to influence the work reported in this paper.

References

[1] K. J. Ardila-Fierro and J. G. Hernández, "Sustainability Assessment of Mechanochemistry by Using the Twelve Principles of Green Chemistry," *ChemSusChem*, vol. 14, no. 10, pp. 2145–2162, 2021, doi: 10.1002/cssc.202100478.

[2] T. Schaub, "Efficient Industrial Organic Synthesis and the Principles of Green Chemistry," *Chemistry - A European Journal*, vol. 27, no. 6, pp. 1865–1869, 2021, doi: 10.1002/chem.202003544.

[3] T. L. Chen, H. Kim, S. Y. Pan, P. C. Tseng, Y. P. Lin, and P. C. Chiang, "Implementation of green chemistry principles in circular economy system towards sustainable development goals: Challenges and perspectives," *Science of the Total Environment*, vol. 716, no. 1, p. 136998, 2020, doi: 10.1016/j.scitotenv.2020.136998.

[4] X. Xie, J. Huo, and H. Zou, "Green process innovation, green product innovation, and corporate financial performance: A content analysis method," *Journal of Business Research*, vol. 101, no. January, pp. 697–706, 2019, doi: 10.1016/j.jbusres.2019.01.010.

[5] I. V. Machado, J. R. N. dos Santos, M. A. P. Januario, and A. G. Corrêa, "Greener organic synthetic methods: Sonochemistry and heterogeneous catalysis promoted multicomponent reactions," *Ultrasonics Sonochemistry*, vol. 78, 2021, doi: 10.1016/j.ultsonch.2021.105704.

[6] K. Okitsu, M. Ashokkumar, and F. Grieser, "Sonochemical synthesis of gold nanoparticles: effects of ultrasound frequency," *The Journal of Physical Chemistry B*, vol. 109, no. 44, pp. 20673–20675, 2005.

[7] S. Asgharzadehahmadi, A. A. A. Raman, R. Parthasarathy, and B. Sajjadi, "Sonochemical reactors: Review on features, advantages and limitations," *Renewable and Sustainable Energy Reviews*, vol. 63, pp. 302–314, 2016.

[8] D. Meroni and C. L. Bianchi, "Ultrasound waves at the service of photocatalysis: From sonochemical synthesis to ultrasound-assisted and piezo-enhanced photocatalysis," *Current Opinion in Green and Sustainable Chemistry*, vol. 36, p. 100639, 2022.

[9] E. M. Modan and A. G. PLĂIAȘU, "Advantages and disadvantages of chemical methods in the elaboration of nanomaterials," *The Annals of "Dunarea de Jos" University of Galati. Fascicle IX, Metallurgy and Materials Science*, vol. 43, no. 1, pp. 53–60, 2020.

[10] D. A. Giannakoudakis, D. Łomot, and J. C. Colmenares, "When sonochemistry meets heterogeneous photocatalysis: designing a sonophotoreactor towards sustainable selective oxidation," *Green Chemistry*, vol. 22, no. 15, pp. 4896–4905, 2020, doi: 10.1039/d0gc00329h.

[11] M. Saidi, A. Benomara, M. Mokhtari, and L. Boukli-Hacene, "Sonochemical synthesis of Zr-fumaric based metal-organic framework (MOF) and its performance evaluation in methyl violet 2B decolorization by photocatalysis," *Reaction Kinetics, Mechanisms and Catalysis*, vol. 131, no. 2, pp. 1009–1021, 2020, doi: 10.1007/s11144-020-01897-3.

[12] A. Panahi, R. Monsef, M. K. Imran, A. A. Mahdi, A. A. Kadhim Ruhaima, and M. Salavati-Niasari, "TmVO4/Fe2O3 nanocomposites: Sonochemical synthesis, characterization, and investigation of photocatalytic activity," *International Journal of Hydrogen Energy*, vol. 48, no. 10, pp. 3916–3930, 2023, doi: 10.1016/j.ijhydene.2022.10.226.

[13] D. F. Dos Santos, A. A. G. Santiago, M. D. Teodoro, F. V. Motta, and M. R. D. Bomio, "Investigation of the photocatalytic and optical properties of the SrMoO4/g-C3N4 heterostructure obtained via sonochemical synthesis with temperature control," *Journal of Environmental Management*, vol. 325, no. PA, p. 116396, 2023, doi: 10.1016/j.jenvman.2022.116396.

[14] M. G. Ashritha *et al.*, "Experimental and computational studies of sonochemical assisted anchoring of carbon quantum dots on reduced graphene oxide sheets towards the photocatalytic activity," *Applied Surface Science*, vol. 545, no. September 2020, p. 148962, 2021, doi: 10.1016/j.apsusc.2021.148962.

[15] C. Wattanawikkam and W. Pecharapa, "Structural studies and photocatalytic properties of Mn and Zn co-doping on TiO2 prepared by single step sonochemical method," *Radiation Physics and Chemistry*, vol. 171, no. January, p. 108714, 2020, doi: 10.1016/j.radphyschem.2020.108714.

[16] L. L. Qian *et al.*, "Sonochemical synthesis and characterization of four nanostructural nickel coordination polymers and photocatalytic degradation of methylene blue," *Ultrasonics Sonochemistry*, vol. 56, no. December 2018, pp. 213–228, 2019, doi: 10.1016/j.ultsonch.2019.04.015.

[17] M. Ali Dheyab, A. Abdul Aziz, M. S. Jameel, P. Moradi Khaniabadi, and B. Mehrdel, "Sonochemical-assisted synthesis of highly stable gold nanoparticles catalyst for decoloration of methylene blue dye," *Inorganic Chemistry Communications*, vol. 127, no. January, p. 108551, 2021, doi: 10.1016/j.inoche.2021.108551.

[18] Á. de J. Ruíz-Baltazar, "Sonochemical activation-assisted biosynthesis of Au/Fe3O4 nanoparticles and sonocatalytic degradation of methyl orange," *Ultrasonics Sonochemistry*, vol. 73, 2021, doi: 10.1016/j.ultsonch.2021.105521.

[19] Z. Talebzadeh, M. Masjedi-Arani, O. Amiri, and M. Salavati-Niasari, "La2Sn2O7/g-C3N4 nanocomposites: Rapid and green sonochemical fabrication and photo-degradation performance for removal of dye contaminations," *Ultrasonics Sonochemistry*, vol. 77, no. July, p. 105678, 2021, doi: 10.1016/j.ultsonch.2021.105678.

[20] S. G. Babu *et al.*, "Synergistic effect of sono-photocatalytic process for the degradation of organic pollutants using CuO-TiO2/rGO," *Ultrasonics Sonochemistry*, vol. 50, no. September 2018, pp. 218–223, 2019, doi: 10.1016/j.ultsonch.2018.09.021.

[21] A. Maroudas, P. K. Pandis, A. Chatzopoulou, L. R. Davellas, G. Sourkouni, and C. Argirusis, "Synergetic decolorization of azo dyes using ultrasounds, photocatalysis and photo-fenton reaction," *Ultrasonics Sonochemistry*, vol. 71, no. September 2020, p. 105367, 2021, doi: 10.1016/j.ultsonch.2020.105367.

[22] Á. de J. Ruíz-Baltazar, "Green synthesis assisted by sonochemical activation of Fe3O4-Ag nano-alloys: Structural characterization and studies of sorption of cationic dyes," *Inorganic Chemistry Communications*, vol. 120, no. July, p. 108148, 2020, doi: 10.1016/j.inoche.2020.108148.

[23] M. Ghiyasiyan-Arani, M. Salavati-Niasari, and S. Naseh, "Enhanced photodegradation of dye in waste water using iron vanadate nanocomposite; ultrasound-assisted preparation and characterization," *Ultrasonics Sonochemistry*, vol. 39, no. May, pp. 494–503, 2017, doi: 10.1016/j.ultsonch.2017.05.025.

[24] J. X. Li, Y. F. Li, L. W. Liu, and G. H. Cui, "Luminescence, electrochemical and photocatalytic properties of sub-micron nickel(II) and cobalt(II) coordination polymers synthesized by sonochemical process," *Ultrasonics Sonochemistry*, vol. 41, no. August 2017, pp. 196–205, 2018, doi: 10.1016/j.ultsonch.2017.09.039.

[25] V. Pavitra, Udayabhanu, R. Harini, R. Viswanatha, B. M. Praveen, and G. Nagaraju, "Sonochemical synthesis of SnO2–CuO nanocomposite: diverse applications on Li-ion battery, electrochemical sensing and photocatalytic activity," *Journal of Materials Science: Materials in Electronics*, vol. 31, no. 11, pp. 8737–8749, 2020, doi: 10.1007/s10854-020-03408-5.

[26] S. Milad Tabatabaeinejad *et al.*, "Sonochemical synthesis and characterization of Ho-Cu-O nanostructures and their application as photocatalyst for degradation of water-soluble organic pollutants under UV light," *Arabian Journal of Chemistry*, vol. 16, no. 6, p. 104768, 2023, doi: 10.1016/j.arabjc.2023.104768.

[27] S. Y. Hao, Y. H. Li, Z. C. Hao, and G. H. Cui, "Sonochemical synthesis of two nanostructured silver(I) coordination polymers based on semi-rigid bis(benzimidazole) ligands," *Ultrasonics Sonochemistry*, vol. 39, no. March, pp. 636–644, 2017, doi: 10.1016/j.ultsonch.2017.04.008.

[28] J. Guo *et al.*, "Sonochemical synthesis of TiO2 nanoparticles on graphene for use as photocatalyst," *Ultrasonics Sonochemistry*, vol. 18, no. 5, pp. 1082–1090, 2011, doi: 10.1016/j.ultsonch.2011.03.021.

[29] M. Dükkanci, M. Vinatoru, and T. J. Mason, "The sonochemical decolourisation of textile azo dye Orange II: Effects of Fenton type reagents and UV light," *Ultrasonics Sonochemistry*, vol. 21, no. 2, pp. 846–853, 2014, doi: 10.1016/j.ultsonch.2013.08.020.

[30] S. E. H. Etaiw, R. S. Farag, H. Marie, and F. A. Elsharqawy, "Crystal structure and sonochemical nanosized synthesizing of diaquo-bis-(pyrazine-2-carboxylato) copper (II) complex: Sensing and photocatalytic activity," *Solid State Sciences*, vol. 102, no. February, p. 106160, 2020, doi: 10.1016/j.solidstatesciences.2020.106160.

[31] K. Qi, C. Zhuang, M. Zhang, P. Gholami, and A. Khataee, "Sonochemical synthesis of photocatalysts and their applications," *Journal of Materials Science and Technology*, vol. 123, pp. 243–256, 2022, doi: 10.1016/j.jmst.2022.02.019.

[32] D. Meroni, R. Djellabi, M. Ashokkumar, C. L. Bianchi, and D. C. Boffito, "Sonoprocessing: From Concepts to Large-Scale Reactors," *Chemical Reviews*, vol. 122, no. 3, pp. 3219–3258, 2022, doi: 10.1021/acs.chemrev.1c00438.

[33] S. R. Pradhan, R. F. Colmenares-Quintero, and J. C. C. Quintero, "Designing microflowreactors for photocatalysis using sonochemistry: A systematic review article," *Molecules*, vol. 24, no. 18, 2019, doi: 10.3390/molecules24183315.

[34] G. Cravotto and P. Cintas, "Power ultrasound in organic synthesis: Moving cavitational chemistry from academia to innovative and large-scale applications," *Chemical Society Reviews*, vol. 35, no. 2, pp. 180–196, 2006, doi: 10.1039/b503848k.

[35] P. Chowdhury and T. Viraraghavan, "Sonochemical degradation of chlorinated organic compounds, phenolic compounds and organic dyes - A review," *Science of the Total Environment*, vol. 407, no. 8, pp. 2474–2492, 2009, doi: 10.1016/j.scitotenv.2008.12.031.

[36] C. Y. Teh, T. Y. Wu, and J. C. Juan, "An application of ultrasound technology in synthesis of titania-based photocatalyst for degrading pollutant," *Chemical Engineering Journal*, vol. 317, pp. 586–612, 2017, doi: 10.1016/j.cej.2017.01.001.

[37] B. T. Y. Wu, N. Guo, C. Y. Teh, and J. X. W. Hay, *Advances in Ultrasound Technology for Environmental Remediation*, Shown. Springer Science & Business Media, 2012, 2012.

[38] H. Destaillats, M. R. Hoffmann, and H. C. Wallace, *Chemical Degradation Methods for Wastes and Pollutants: Environmental and Industrial Applications*. CRC Press, 2003, 2003.

[39] D. G. Shchukin, E. Skorb, V. Belova, and H. Möhwald, "Ultrasonic cavitation at solid surfaces," *Advanced Materials*, vol. 23, no. 17, pp. 1922–1934, 2011, doi: 10.1002/adma.201004494.

[40] H. A. Choudhury, A. Choudhary, M. Sivakumar, and V. S. Moholkar, "Mechanistic investigation of the sonochemical synthesis of zinc ferrite," *Ultrasonics Sonochemistry*, vol. 20, no. 1, pp. 294–302, 2013, doi: 10.1016/j.ultsonch.2012.06.006.

[41] X. Hangxun, B. W. Zeiger, and K. S. Suslick, "Sonochemical synthesis of nanomaterials," *Chemical Society Reviews*, vol. 42, no. 7, pp. 2555–2567, 2013, doi: 10.1039/c2cs35282f.

[42] N. Pokhrel, P. K. Vabbina, and N. Pala, "Sonochemistry: Science and Engineering," *Ultrasonics Sonochemistry*, vol. 29, pp. 104–128, 2016, doi: 10.1016/j.ultsonch.2015.07.023.

[43] N. Brezhneva, E. V. Skorb, and S. A. Ulasevich, "Titanium surface nanostructuring by high-intensity ultrasound," *Proceedings of the 2017 IEEE 7th International Conference on Nanomaterials: Applications and Properties, NAP 2017*, vol. 2017-Janua, pp. 7–12, 2017, doi: 10.1109/NAP.2017.8190201.

[44] S. R. Yousefi, O. Amiri, and M. Salavati-Niasari, "Control sonochemical parameter to prepare pure Zn0.35Fe2.65O4 nanostructures and study their photocatalytic activity," *Ultrasonics Sonochemistry*, vol. 58, no. May, p. 104619, 2019, doi: 10.1016/j.ultsonch.2019.104619.

[45] Y. M. Hunge, A. A. Yadav, S. Liu, and V. L. Mathe, "Sonochemical synthesis of CZTS photocatalyst for photocatalytic degradation of phthalic acid," *Ultrasonics Sonochemistry*, vol. 56, no. April, pp. 284–289, 2019, doi: 10.1016/j.ultsonch.2019.04.003.

[46] R. Hernández *et al.*, "Au-tio2 synthesized by a microwave-and sonochemistry-assisted sol-gel method: Characterization and application as photocatalyst," *Catalysts*, vol. 10, no. 9, pp. 1–18, 2020, doi: 10.3390/catal10091052.

[47] M. A. Dheyab, A. A. Aziz, M. S. Jameel, P. M. Khaniabadi, and B. Mehrdel, "Mechanisms of effective gold shell on Fe3O4 core nanoparticles formation using sonochemistry method," *Ultrasonics Sonochemistry*, vol. 64, no. October 2019, p. 104865, 2020, doi: 10.1016/j.ultsonch.2019.104865.

[48] H.-M. Kim, C.-H. Lee, and B. Kim, "Sonochemical synthesis of silica particles and their size control," *Applied Surface Science*, vol. 380, pp. 305–308, Sep. 2016, doi: 10.1016/j.apsusc.2015.12.048.

[49] H. E. Hansen, F. Seland, S. Sunde, O. S. Burheim, and B. G. Pollet, "Two routes for sonochemical synthesis of platinum nanoparticles with narrow size distribution," *Mater. Adv.*, vol. 2, no. 6, pp. 1962–1971, 2021, doi: 10.1039/D0MA00909A.

[50] Q. Wang *et al.*, "Synthesis of (ZrO2-Al2O3)/GO nanocomposite by sonochemical method and the mechanism analysis of its high defluoridation," *Journal of Hazardous Materials*, vol. 381, no. January 2019, p. 120954, 2020, doi: 10.1016/j.jhazmat.2019.120954.

[51] D. A. Giannakoudakis *et al.*, "Ultrasound-assisted decoration of CuOx nanoclusters on TiO2 nanoparticles for additives free photocatalytic hydrogen production and biomass valorization by selective oxidation," *Molecular Catalysis*, vol. 514, 2021, doi: 10.1016/j.mcat.2021.111664.

[52] J. A. Fuentes-García, J. Santoyo-Salzar, E. Rangel-Cortes, G. F. Goya, V. Cardozo-Mata, and J. A. Pescador-Rojas, "Effect of ultrasonic irradiation power on sonochemical synthesis of gold nanoparticles," *Ultrasonics Sonochemistry*, vol. 70, no. April 2020, p. 105274, 2021, doi: 10.1016/j.ultsonch.2020.105274.

[53] M. Mousavi-Kamazani and F. Azizi, "Facile sonochemical synthesis of Cu doped CeO2 nanostructures as a novel dual-functional photocatalytic adsorbent," *Ultrasonics Sonochemistry*, vol. 58, no. May, p. 104695, 2019, doi: 10.1016/j.ultsonch.2019.104695.

[54] A. Bahadoran, M. Farhadian, G. Hoseinzadeh, and Q. Liu, "Novel flake-like Z-Scheme Bi2WO6-ZnBi2O4 heterostructure prepared by sonochemical assisted hydrothermal procedures with enhanced visible-light photocatalytic activity," *Journal of Alloys and Compounds*, vol. 883, p. 160895, 2021, doi: 10.1016/j.jallcom.2021.160895.

[55] F. Zhang *et al.*, "Recent advances and applications of semiconductor photocatalytic technology," *Applied Sciences (Switzerland)*, vol. 9, no. 12, 2019, doi: 10.3390/app9122489.

[56] Y. Nagata, Y. Watananabe, S. Fujita, T. Dohmaru, and S. Taniguchi, "Formation of colloidal silver in water by ultrasonic irradiation," *Journal of the Chemical Society, Chemical Communications*, no. 21, pp. 1620–1622, 1992.

[57] M. Kubo, K. Matsuoka, A. Takahashi, N. Shibasaki-Kitakawa, and T. Yonemoto, "Kinetics of ultrasonic degradation of phenol in the presence of TiO2 particles," *Ultrasonics sonochemistry*, vol. 12, no. 4, pp. 263–269, 2005.

[58] F. Ahmedchekkat, M. S. Medjram, M. Chiha, and A. M. A. Al-Bsoul, "Sonophotocatalytic degradation of Rhodamine B using a novel reactor geometry: Effect of operating conditions," *Chemical Engineering Journal*, vol. 178, pp. 244–251, 2011.

[59] Y. He, F. Grieser, and M. Ashokkumar, "Kinetics and mechanism for the sonophotocatalytic degradation of p-chlorobenzoic acid," *The Journal of Physical Chemistry A*, vol. 115, no. 24, pp. 6582–6588, 2011.

[60] S. Anju, S. Yesodharan, and E. Yesodharan, "Zinc oxide mediated sonophotocatalytic degradation of phenol in water," *Chemical Engineering Journal*, vol. 189, pp. 84–93, 2012.

[61] N. B. Bokhale *et al.*, "Sonocatalytic and sonophotocatalytic degradation of rhodamine 6G containing wastewaters," *Ultrasonics sonochemistry*, vol. 21, no. 5, pp. 1797–1804, 2014.

[62] I. Michael *et al.*, "Proposed transformation pathway and evolution profile of diclofenac and ibuprofen transformation products during (sono) photocatalysis," *Applied Catalysis B: Environmental*, vol. 147, pp. 1015–1027, 2014.

[63] P. Nuengmatcha, S. Chanthai, R. Mahachai, and W.-C. Oh, "Sonocatalytic performance of ZnO/graphene/TiO2 nanocomposite for degradation of dye pollutants (methylene blue, texbrite BAC-L, texbrite BBU-L and texbrite NFW-L) under ultrasonic irradiation," *Dyes and Pigments*, vol. 134, pp. 487–497, 2016.

[64] B. Bhanvase, T. Shende, and S. Sonawane, "A review on graphene–TiO2 and doped graphene–TiO2 nanocomposite photocatalyst for water and wastewater treatment," *Environmental Technology Reviews*, vol. 6, no. 1, pp. 1–14, 2017.

[65] D. Panda and S. Manickam, "Recent advancements in the sonophotocatalysis (SPC) and doped-sonophotocatalysis (DSPC) for the treatment of recalcitrant hazardous organic water pollutants," *Ultrasonics sonochemistry*, vol. 36, pp. 481–496, 2017.

[66] J. Y. Lee and J. H. Choi, "Sonochemical synthesis of Ce-doped TiO2 nanostructure: A visible-light-driven photocatalyst for degradation of toluene and O-Xylene," *Materials*, vol. 12, no. 8, 2019, doi: 10.3390/ma12081265.

[67] M. D. Purkayastha *et al.*, "Sonochemical synthesis of nanospherical TiO2 within graphene oxide nanosheets and its application as a photocatalyst and a Schottky diode," *FlatChem*, vol. 22, no. April, p. 100180, 2020, doi: 10.1016/j.flatc.2020.100180.

[68] A. Dey and P. R. Gogate, "Ultrasound assisted synthesis of Fe-TiO2 and Ce-TiO2 catalysts and subsequent application for photocatalytic, sonocatalytic, and sonophotocatalytic decolorization of basic Victoria blue dye," *Environmental Quality Management*, no. January, pp. 1–15, 2023, doi: 10.1002/tqem.21970.

[69] A. Dey, S. Korde, P. R. Gogate, and C. Agarkoti, "Sonochemical synthesis of Ce-TiO2 nanocatalyst and subsequent application for treatment of real textile industry effluent," *Ultrasonics Sonochemistry*, vol. 96, no. March, p. 106426, 2023, doi: 10.1016/j.ultsonch.2023.106426.

[70] O. Oloye, J. F. S. Fernando, D. Golberg, and A. P. O'Mullane, "Sonochemical Synthesis of Ga/ZnO Nanomaterials from a Liquid Metal for Photocatalytic Applications," *Advanced Sustainable Systems*, vol. 6, no. 1, pp. 1–7, 2022, doi: 10.1002/adsu.202100312.

[71] A. Muthukrishnaraj, S. S. Kalaivani, A. Manikandan, H. P. Kavitha, R. Srinivasan, and N. Balasubramanian, "Sonochemical synthesis and visible light induced photocatalytic property of reduced graphene oxide@ZnO hexagonal hollow rod nanocomposite," *Journal of Alloys and Compounds*, vol. 836, p. 155377, 2020, doi: 10.1016/j.jallcom.2020.155377.

[72] P. Intaphong *et al.*, "Sonochemical Synthesis of Pd Nanoparticle/ZnO Flower Photocatalyst Used for Methylene Blue and Methyl Orange Degradation under UV Radiation," *Russian Journal of Inorganic Chemistry*, vol. 66, no. 14, pp. 2123–2133, 2021, doi: 10.1134/S0036023621140047.

[73] S. Shenoy, S. Ahmed, I. M. C. Lo, S. Singh, and K. Sridharan, "Rapid sonochemical synthesis of copper doped ZnO grafted on graphene as a multi-component hierarchically structured visible-light-driven photocatalyst," *Materials Research Bulletin*, vol. 140, no. September 2020, p. 111290, 2021, doi: 10.1016/j.materresbull.2021.111290.

[74] A. Singh, R. Manivannan, and S. Noyel Victoria, "Simple one-pot sonochemical synthesis of copper sulphide nanoparticles for solar cell applications," *Arabian Journal of Chemistry*, vol. 12, no. 8, pp. 2439–2447, 2019, doi: 10.1016/j.arabjc.2015.03.013.

[75] Y. Li *et al.*, "Metal Chalcogenides with Heterostructures for High-Performance Rechargeable Batteries," *Small Science*, vol. 1, no. 9, p. 2100012, 2021, doi: 10.1002/smsc.202100012.

[76] K. Hedayati, D. Ghanbari, M. Kord, and M. Goodarzi, "(Co, Ag, Ni, Cd, Mn, Cr)-doped PbS photo-catalyst: sonochemical-assisted synthesis of magnetite nanocomposites applicable for elimination of toxic pollutants," *Journal of Materials Science: Materials in Electronics*, vol. 32, no. 1, pp. 373–383, 2021, doi: 10.1007/s10854-020-04787-5.

[77] K. Patel, A. Patel, and V. P. Jethwa, *Sonochemically exfoliation and photodetection properties of Cu0.2Sn0.8Se nanoparticles*. 2021.

[78] N. Singh and M. Taunk, "Structural, Optical, and Electrical Studies of Sonochemically Synthesized CuS Nanoparticles," *Semiconductors*, vol. 54, no. 9, pp. 1016–1022, 2020, doi: 10.1134/S1063782620090262.

[79] F. Monjezi, F. Jamali-Sheini, and R. Yousefi, "Ultrasound-assisted electrodeposition of Cu3Se2 nanosheets and efficient solar cell performance," *Journal of Alloys and Compounds*, vol. 780, pp. 626–633, 2019, doi: 10.1016/j.jallcom.2018.11.267.

[80] N. Hoda and F. Jamali-Sheini, "Influence of synthesis parameters on the physical properties of Cu3Se2 nanostructures using the sonochemical method," *Ceramics International*, vol. 45, no. 14, pp. 16765–16775, 2019, doi: 10.1016/j.ceramint.2019.05.212.

[81] P. Sakthi, J. Uma, C. Siva, and B. Balraj, "Sonochemical synthesis of interconnected SnS nanocrystals for supercapacitor and solar-physical conversion applications," *Optical Materials*, vol. 132, no. August, p. 112759, 2022, doi: 10.1016/j.optmat.2022.112759.

[82] A. J. Khimani, S. H. Chaki, R. K. Giri, R. R. Meena, R. M. Kannaujiya, and M. P. Deshpande, "Thermal exploration of sonochemically achieved SnS2 nanoparticles: Elemental, structural, and morphological investigations of TG residual SnS2," *Chemical Thermodynamics and Thermal Analysis*, vol. 9, no. January, pp. 4–11, 2023, doi: 10.1016/j.ctta.2023.100104.

[83] A. Jafarinejad, H. Bashiri, and M. Salavati-Niasari, "Sonochemical synthesis and characterization of CuInS2 nanostructures using new sulfur precursor and their application as photocatalyst for degradation of organic pollutants under simulated sunlight," *Arabian Journal of Chemistry*, vol. 15, no. 8, p. 104007, 2022, doi: 10.1016/j.arabjc.2022.104007.

[84] X. Yang, Y. Zhou, and J. He, "Two unexplored two-dimensional MSe2 (M = Cd, Zn) structures as the photocatalysts of water splitting and the enhancement of their performances by strain," *Vacuum*, vol. 182, no. June, p. 109728, 2020, doi: 10.1016/j.vacuum.2020.109728.

[85] M. Politi *et al.*, "A high-throughput workflow for the synthesis of CdSe nanocrystals using a sonochemical materials acceleration platform," *Digital Discovery*, 2023, doi: 10.1039/d3dd00033h.

[86] M. Zargarpour, F. Jamali-Sheini, and M. Cheraghizade, "Sonochemical synthesis of Fe-doped Cu3Se2 nanoparticles: Correlation of the strain and electrical properties for optoelectronics applications," *Advanced Powder Technology*, vol. 32, no. 10, pp. 3412–3424, 2021, doi: 10.1016/j.apt.2021.07.020.

[87] G. Matyszczak *et al.*, "Sonochemical preparation of SnS and SnS2 nano- and micropowders and their characterization," *Ultrasonics Sonochemistry*, vol. 75, no. April, pp. 0–9, 2021, doi: 10.1016/j.ultsonch.2021.105594.

[88] M. Geravand and F. Jamali-Sheini, "Synthesis and physical properties of un- and Zn-doped Ag2S nanoparticles," *Advanced Powder Technology*, vol. 30, no. 2, pp. 347–358, 2019, doi: 10.1016/j.apt.2018.11.012.

[89] H. Yang, "A short review on heterojunction photocatalysts: Carrier transfer behavior and photocatalytic mechanisms," *Materials Research Bulletin*, vol. 142, no. April, p. 111406, 2021, doi: 10.1016/j.materresbull.2021.111406.

[90] N. F. Andrade Neto, A. B. Lima, R. R. Y. O. V. Wilson, T. C. N. Nicacio, M. R. D. Bomio, and F. V. Motta, "Heterostructures obtained by ultrasonic methods for photocatalytic application: A review," *Materials Science in Semiconductor Processing*, vol. 139, no. April 2021, p. 106311, 2022, doi: 10.1016/j.mssp.2021.106311.

[91] Parul, K. Kaur, R. Badru, P. P. Singh, and S. Kaushal, "Photodegradation of organic pollutants using heterojunctions: A review," *Journal of Environmental Chemical Engineering*, vol. 8, no. 2, p. 103666, 2020, doi: 10.1016/j.jece.2020.103666.

[92] L. Guo *et al.*, "Morphology engineering of type-II heterojunction nanoarrays for improved sonophotocatalytic capability," *Ultrasonics Sonochemistry*, vol. 81, p. 105849, 2021, doi: 10.1016/j.ultsonch.2021.105849.

[93] E. H. Hashem, A. Fahmy, A. Abbas, M. Tarek, B. Mahran, and M. A. Ahmed, "Fabrication of novel AgIO4/TiO2 heterojunction for photocatalytic hydrogen production through direct Z-scheme mechanism," *Nanotechnology for Environmental Engineering*, vol. 5, no. 2, pp. 1–11, 2020, doi: 10.1007/s41204-020-00081-1.

[94] I. Khan and A. Qurashi, "Sonochemical-Assisted in Situ Electrochemical Synthesis of Ag/α-Fe2O3/TiO2 Nanoarrays to Harness Energy from Photoelectrochemical Water Splitting," *ACS Sustainable Chemistry and Engineering*, vol. 6, no. 9, pp. 11235–11245, 2018, doi: 10.1021/acssuschemeng.7b02848.

[95] M. Benaissa *et al.*, "BiVO3/g-C3N4 S-scheme heterojunction nanocomposite photocatalyst for hydrogen production and amaranth dye removal," *Optical Materials*, vol. 118, no. March, p. 111237, 2021, doi: 10.1016/j.optmat.2021.111237.

[96] M. Nawaz *et al.*, "Sonochemical synthesis of ZnCo2O4/Ag3PO4 heterojunction photocatalysts for the degradation of organic pollutants and pathogens: a combined experimental and computational study," *New Journal of Chemistry*, vol. 46, no. 29, pp. 14030–14042, 2022, doi: 10.1039/d2nj01352e.

[97] H. S. M. Abd-Rabboh, M. Benaissa, M. S. Hamdy, M. A. Ahmed, and M. Glal, "Synthesis of an efficient, and recyclable mesoporous BiVO4/TiO2 direct Z-scheme heterojunction by sonochemical route for photocatalytic hydrogen production and photodegradation of rhodamine B dye in the visible region," *Optical Materials*, vol. 114, no. October 2020, p. 110761, 2021, doi: 10.1016/j.optmat.2020.110761.

[98] A. R. Mahammed Shaheer *et al.*, "Sonochemical assisted impregnation of Bi2WO6 on TiO2 nanorod to form Z-scheme heterojunction for enhanced photocatalytic H2 production," *Advanced Powder Technology*, vol. 32, no. 12, pp. 4734–4743, 2021, doi: 10.1016/j.apt.2021.10.022.

[99] K. Kaviyarasan, V. Vinoth, T. Sivasankar, A. M. Asiri, J. J. Wu, and S. Anandan, "Photocatalytic and photoelectrocatalytic performance of sonochemically synthesized Cu2O@TiO2 heterojunction nanocomposites," *Ultrasonics Sonochemistry*, vol. 51, no. June 2018, pp. 223–229, 2019, doi: 10.1016/j.ultsonch.2018.10.022.

[100] Z. K. Heiba, M. A. Ahmed, M. Hassan, A. Badawi, A. M. El-naggar, and M. B. Mohamed, "Sonochemical synthesis of Ag2CO3/CeO2 p-n heterojunction for decomposition of rhodamine B dye," *Optical Materials*, vol. 141, no. March, p. 113945, 2023, doi: 10.1016/j.optmat.2023.113945.

[101] A. Alsalme, A. AlFawaz, A. H. Glal, M. F. Abdel Messih, A. Soltan, and M. A. Ahmed, "S-scheme AgIO4/CeO2 heterojunction nanocomposite photocatalyst for degradation of rhodamine B dye," *Journal of Photochemistry and Photobiology A: Chemistry*, vol. 439, no. January, 2023, doi: 10.1016/j.jphotochem.2023.114596.

[102] V. Ramasamy Raja, A. Karthika, S. Lok Kirubahar, A. Suganthi, and M. Rajarajan, "Sonochemical synthesis of novel ZnFe 2 O 4 /CeO 2 heterojunction with highly enhanced visible light photocatalytic activity," *Solid State Ionics*, vol. 332, no. January, pp. 55–62, 2019, doi: 10.1016/j.ssi.2018.12.016.

[103] S. Asgharzadehahmadi, A. A. Abdul Raman, R. Parthasarathy, and B. Sajjadi, "Sonochemical reactors: Review on features, advantages and limitations," *Renewable and Sustainable Energy Reviews*, vol. 63, pp. 302–314, 2016, doi: 10.1016/j.rser.2016.05.030.

[104] D. Meroni, R. Djellabi, M. Ashokkumar, C. L. Bianchi, and D. C. Boffito, "Sonoprocessing: From Concepts to Large-Scale Reactors," *Chemical Reviews*, vol. 122, no. 3, pp. 3219–3258, 2022, doi: 10.1021/acs.chemrev.1c00438.

[105] A. P. U. S. Kuhn, Z. Dong, C. Delacour, K. Carogher, "Continuous Ultrasonic Reactors : Design , Mechanism," *Material Science and Engineering*, vol. 13, p. 344, 2020.

[106] D. P. Kale, S. P. Deshmukh, S. R. Shirsath, and B. A. Bhanvase, "Sonochemical preparation of multifunctional rGO-ZnS-TiO2 ternary nanocomposite and its application for CV dye removal," *Optik*, vol. 208, no. December 2019, p. 164532, 2020, doi: 10.1016/j.ijleo.2020.164532.

[107] V. D. Potle, S. R. Shirsath, B. A. Bhanvase, and V. K. Saharan, "Sonochemical preparation of ternary rGO-ZnO-TiO2 nanocomposite photocatalyst for efficient degradation of crystal violet dye," *Optik*, vol. 208, no. December 2019, 2020, doi: 10.1016/j.ijleo.2020.164555.

[108] E. Luévano-Hipólito and L. M. Torres-Martínez, "Sonochemical synthesis of ZnO nanoparticles and its use as photocatalyst in H2 generation," *Materials Science and Engineering B: Solid-State Materials for Advanced Technology*, vol. 226, no. September, pp. 223–233, 2017, doi: 10.1016/j.mseb.2017.09.023.

[109] D. Schieppati, F. Galli, M. L. Peyot, V. Yargeau, C. L. Bianchi, and D. C. Boffito, "An ultrasound-assisted photocatalytic treatment to remove an herbicidal pollutant from wastewaters," *Ultrasonics Sonochemistry*, vol. 54, no. January, pp. 302–310, 2019, doi: 10.1016/j.ultsonch.2019.01.027.

[110] M. Chen, K. Zhuang, J. Sui, C. Sun, Y. Song, and N. Jin, "Hydrodynamic cavitation-enhanced photocatalytic activity of P-doped TiO2 for degradation of ciprofloxacin:

Synergetic effect and mechanism," *Ultrasonics Sonochemistry*, vol. 92, no. December 2022, p. 106265, 2023, doi: 10.1016/j.ultsonch.2022.106265.

[111] S. R. Yashas *et al.*, "Sonochemical synthesis of graphitic carbon nitride-manganese oxide interfaces for enhanced photocatalytic degradation of tetracycline hydrochloride," *Environmental Science and Pollution Research*, vol. 28, no. 4, pp. 4778–4789, 2021, doi: 10.1007/s11356-020-10813-0.

[112] H. Gu, X. Chen, F. Chen, X. Zhou, and Z. Parsaee, "Ultrasound-assisted biosynthesis of CuO-NPs using brown alga Cystoseira trinodis: Characterization, photocatalytic AOP, DPPH scavenging and antibacterial investigations," *Ultrasonics Sonochemistry*, vol. 41, no. July 2017, pp. 109–119, 2018, doi: 10.1016/j.ultsonch.2017.09.006.

[113] C. Palacio *et al.*, "Influence of organic acids on the phases and physical characteristics of titanium dioxide synthesized by sol–gel for air depollution through heterogeneous photocatalysis," *Journal of Chemical Technology and Biotechnology*, vol. 97, no. 11, pp. 2994–3000, 2022, doi: 10.1002/jctb.7052.

[114] S. Mosleh, M. R. Rahimi, M. Ghaedi, K. Dashtian, and S. Hajati, "Sonochemical-assisted synthesis of CuO/Cu2O/Cu nanoparticles as efficient photocatalyst for simultaneous degradation of pollutant dyes in rotating packed bed reactor: LED illumination and central composite design optimization," *Ultrasonics Sonochemistry*, vol. 40, no. August 2017, pp. 601–610, 2018, doi: 10.1016/j.ultsonch.2017.08.007.

[115] A. Miri and F. Ghorbani, "Syntheses of Ag[Cu@Ag]\APTMS\boehmite as a photocatalyst for methylene blue degradation in batch and continuous flow systems under visible light," *Environmental Nanotechnology, Monitoring and Management*, vol. 16, no. January, p. 100493, 2021, doi: 10.1016/j.enmm.2021.100493.

[116] G. Fan *et al.*, "Design of continuous flow membrane reactor for in-situ sonophotocatalytic degradation of ciprofloxacin," *Journal of Environmental Chemical Engineering*, vol. 10, no. 6, p. 108888, 2022, doi: 10.1016/j.jece.2022.108888.

[117] S. Mosleh, M. R. Rahimi, M. Ghaedi, and K. Dashtian, "Sonophotocatalytic degradation of trypan blue and vesuvine dyes in the presence of blue light active photocatalyst of Ag3PO4/Bi2S3-HKUST-1-MOF: Central composite optimization and synergistic effect study," *Ultrasonics Sonochemistry*, vol. 32, pp. 387–397, 2016, doi: 10.1016/j.ultsonch.2016.04.007.

[118] B. Palanisamy, B. Paul, and C. H. Chang, "The synthesis of cadmium sulfide nanoplatelets using a novel continuous flow sonochemical reactor," *Ultrasonics Sonochemistry*, vol. 26, pp. 452–460, 2015, doi: 10.1016/j.ultsonch.2015.01.004.

[119] S. Abdolhosseinzadeh, M. Mousavi, N. Haghmoradi, and S. A. Gürsel, "A continuous-flow photocatalytic reactor for the precisely controlled deposition of metallic nanoparticles," *Journal of Visualized Experiments*, vol. 2019, no. 146, pp. 1–8, 2019, doi: 10.3791/58883.

[120] Z. Dong, S. D. A. Zondag, M. Schmid, Z. Wen, and T. Noël, "A meso-scale ultrasonic milli-reactor enables gas–liquid-solid photocatalytic reactions in flow," *Chemical*

Engineering Journal, vol. 428, no. February 2021, 2022, doi: 10.1016/j.cej.2021.130968.

[121] A. V. Abramova *et al.*, "A sol-gel method for applying nanosized antibacterial particles to the surface of textile materials in an ultrasonic field," *Ultrasonics Sonochemistry*, vol. 60, no. October 2018, p. 104788, 2020, doi: 10.1016/j.ultsonch.2019.104788.

[122] I. M. Khokhawala and P. R. Gogate, "Degradation of phenol using a combination of ultrasonic and UV irradiations at pilot scale operation," *Ultrasonics Sonochemistry*, vol. 17, no. 5, pp. 833–838, 2010, doi: 10.1016/j.ultsonch.2010.02.012.

[123] J. C. Colmenares, V. Nair, E. Kuna, and D. Łomot, "Development of photocatalyst coated fluoropolymer based microreactor using ultrasound for water remediation," *Ultrasonics Sonochemistry*, vol. 41, no. September 2017, pp. 297–302, 2018, doi: 10.1016/j.ultsonch.2017.09.053.

[124] V. Katoch *et al.*, "Microflow synthesis and enhanced photocatalytic dye degradation performance of antibacterial Bi2O3 nanoparticles," *Environmental Science and Pollution Research*, vol. 28, no. 15, pp. 19155–19165, 2021, doi: 10.1007/s11356-020-11711-1.

[125] V. Nair, J. C. Colmenares, and D. Lisovytskiy, "Ultrasound assisted ZnO coating in a microflow based photoreactor for selective oxidation of benzyl alcohol to benzaldehyde," *Green Chemistry*, vol. 21, no. 6, pp. 1241–1246, 2019, doi: 10.1039/c8gc03131b.

[126] H. Zhu, K. J. Wu, and C. H. He, "Ultrasound-assisted synthesis of visible-light-driven Ag/g-C3N4 catalysts in a continuous flow reactor," *Chemical Engineering Journal*, vol. 429, no. September 2021, p. 132412, 2022, doi: 10.1016/j.cej.2021.132412.

[127] Ö. Tuna, Ş. Karadirek, and E. B. Simsek, "Deposition of CaFe2O4 and LaFeO3 perovskites on polyurethane filter: A new photocatalytic support for flowthrough degradation of tetracycline antibiotic," *Environmental Research*, vol. 205, no. May 2021, 2022, doi: 10.1016/j.envres.2021.112389.

[128] S. R. Pradhan, V. Nair, D. A. Giannakoudakis, D. Lisovytskiy, and J. C. Colmenares, "Design and development of TiO2 coated microflow reactor for photocatalytic partial oxidation of benzyl alcohol," *Molecular Catalysis*, vol. 486, no. February, p. 110884, 2020, doi: 10.1016/j.mcat.2020.110884.

[129] X. Yao, Y. Zhang, L. Du, J. Liu, and J. Yao, "Review of the applications of microreactors," *Renewable and Sustainable Energy Reviews*, vol. 47, pp. 519–539, Jul. 2015, doi: 10.1016/j.rser.2015.03.078.

[130] D. Chandrasekhar, S. Borra, J. S. Kapure, G. S. Shivaji, G. Srinivasulu, and R. A. Maurya, "Visible-light photoredox catalysis: direct synthesis of fused β-carbolines through an oxidation/[3+ 2] cycloaddition/oxidative aromatization reaction cascade in batch and flow microreactors," *Organic Chemistry Frontiers*, vol. 2, no. 10, pp. 1308–1312, 2015.

[131] Y. Matsushita *et al.*, "Recent progress on photoreactions in microreactors," *Pure and Applied Chemistry*, vol. 79, no. 11, pp. 1959–1968, 2007.

[132] M. Oelgemoeller, "Highlights of photochemical reactions in microflow reactors," *Chemical engineering & technology*, vol. 35, no. 7, pp. 1144–1152, 2012.

[133] O. Pandoli, T. D. Rosso, V. M. Santos, R. de S. Rezende, and B. A. Marinkovic, "Prototyping of photocatalytic microreactor and testing of photodegradation of organic dye," *Química Nova*, vol. 38, pp. 859–863, 2015.

- Sonochemical synthesis of photocatalysts is a promising green field for the removal of toxic substances.
- Sonochemistry affects the structure of the synthesized nanoparticles in favour of photocatalytic experiments.
- Batch and continuous flow reactors are the most studied systems.
- Continuous flow reactors are used both for the synthesis and the photocatalytic experiments.
- Microflow reactors offer commercial-scale advantages.